AUSTRALIAN MUSEUM SCIENTIFIC PUBLICATIONS

Sutherland, F. L., D. F. Hendry, B. J. Barron, W. L. Matthews and J. D. Hollis, 1996. An unusual Tasmanian Tertiary basalt sequence, near Boat Harbour, northwest Tasmania. *Records of the Australian Museum* 48(2): 131–161. [18 September 1996].

doi:10.3853/j.0067-1975.48.1996.285

ISSN 0067-1975

Published by the Australian Museum, Sydney

Records of the Australian Museum (1996) Vol. 48: 131–161. ISSN 0067-1975

An Unusual Tasmanian Tertiary Basalt Sequence, Near Boat Harbour, Northwest Tasmania

F.L. SUTHERLAND,[1] D.F. HENDRY,[2*] B.J. BARRON,[1]
W.L. MATTHEWS[3] AND J.D. HOLLIS[1]

[1] Division of Earth and Environmental Sciences,
The Australian Museum, 6 College Street, Sydney NSW 2000, Australia
Internet: lins@amsg.AustMus.gov.au
[2] Department of Geology and Geophysics, The University of Sydney NSW 2006, Australia
[3] Department of Mines, PO Box 56, Rosny Park TAS 7018, Australia
* Present address: 16 Sunnyside Street, Gladesville NSW 2111, Australia

ABSTRACT. The mineralogy and petrology of basalts near Boat Harbour, NW Tasmania, are described as this sequence is unusual for Tasmanian Tertiary basalts. The rocks are more sodic and evolved basalts carry more prolific anorthoclase and zircon megacrysts than is normal in Tasmania. Older nephelinites and melilite-nephelinites (26–27 Ma) and younger nepheline hawaiites and mugearites (14–15 Ma) are present and fission track zircon ages (13–14 Ma and 8–9 Ma) demonstrate that zircon was erupted during and after the evolved basalts. The nephelinites and some evolved basalts carry common spinel lherzolite xenoliths, some with rare alkaline reaction veins. Crustal xenoliths are ubiquitous as Precambrian country rocks but include rare 2-pyroxene granulite and anorthosite. Some nephelinites show mariolitic assemblages of olivine, diopside-augite-aegirine clinopyroxenes, nepheline, sodalite, barian sanidine, ulvospinel, titanian richterite, titanian phlogopite and carbonate.

The nephelinites and melilite nephelinite represent primary melts, while the evolved basalts can produce primary basanites by addition of a cumulate wehrlite mineralogy. However, crystal fractionation models for evolving these melts only give inadequate solutions. The low Zr contents, and presence of zircon and anorthoclase megacrysts do not fit into fractionation processes.

Nephelinitic geochemistry indicates 4–7% degrees of partial melting of an amphibole-dominated metasomatised garnet peridotite. Low H_2O+CO_2 contents favour melilite nephelinite melt derived from deeper levels than for the nephelinite melts. Evolved basalts from such metasomatised sources may mark limited fractional crystallisation, while minor early initial melting may produce sodic Zr-rich felsic melts that crystallise anorthoclase and zircon without significant fractionation.

The rocks show an isotopic HIMU imprint, but unlike older east Tasmanian basalts lack trace element signatures related to the Tasman Balleny plume system.

SUTHERLAND, F.L., D.F. HENDRY, B.J. BARRON, W.L. MATTHEWS & J.D. HOLLIS, 1996. An unusual Tasmanian Tertiary basalt sequence, near Boat Harbour, northwest Tasmania. Records of the Australian Museum 48(2): 131–161.

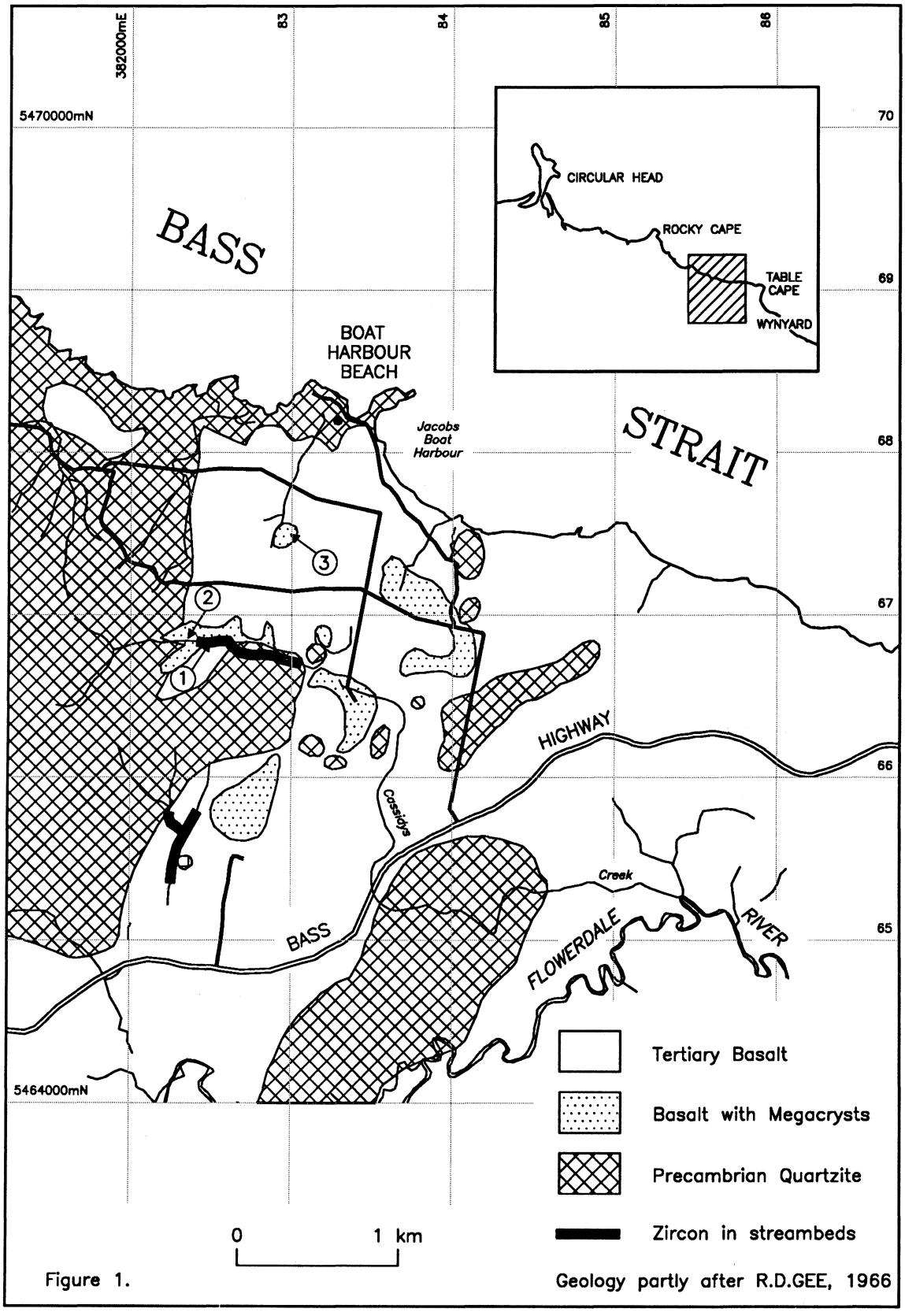

Fig. 1. Map of the Boat Harbour area showing distribution of zircon sites, basalts and basement rocks in the Cassidys Creek region. Circled numbers refer to dated sites: 1 zircon fission track site, 2. olivine melilite nephelinite-olivine nephelinite site, 3 nepheline mugearite site.

The Tertiary basalts exposed in Cassidys Creek near Boat Harbour, NW Tasmania, are unusual among Tasmanian sequences in containing:

1 Olivine melilite nephelinites and nephelinites at the same site

2 evolved alkaline basalts containing conspicuous anorthoclase megacrysts

3 gem zircon suites weathering from some evolved basalts.

The drainages that shed gem zircons from the basalt sequence include Cassidys and Sisters Creeks inland from Boat Harbour (Fig. 1). These creeks drain folded quartzose metasediments of the Proterozoic Rocky Cape Group and overlying Cainozoic gravels and basalts (Gee, 1971). The gem zircons are concentrated within alluvial deposits and were originally thought to come from sub-basaltic gravels, quartzites or a granitic source remote from the area (Matthews, 1973). However, their extraordinary abundance and many practically unabraded crystals suggest a local source (Hollis & Sutherland, 1985). Panning of heavy minerals from weathered, but *in situ* basalts in Upper Cassidys Creek (previously named Shekelton Creek) during this study confirmed a basaltic source for the zircons.

This study concentrates on the basalt sequence and the detailed gemmology, geochemistry and isotope dating of the zircons will be presented elsewhere.

General Volcanic Setting

Volcanic sequences in this area are well exposed only in coastal cliffs between Boat Harbour and Wynyard to the east. Here, undated flows occupy valleys, some of which were filled with lavas before deposition of fossiliferous Late Oligocene/Early Miocene marine beds east of Table Cape (i.e. before 25–26 Ma; Sutherland & Wellman, 1986). These are largely alkaline basalts and some carry anorthoclase megacrysts (Geeves, 1982). Flow foot breccias and largely weathered flows overlie the Early Miocene marine beds east of Table Cape and are mostly alkali basaltic in character. Table Cape itself is a massive teschenite over 170m thick formed by differentiation of a basanite flow and contains abundant peridotitic mantle xenoliths towards the base and common pegmatitic schlieren in the upper parts (Gee, 1971; Geeves, 1982). This flow overlies basal vitric pyroclastics of olivine nephelinite composition, which carry a range of high pressure mantle and lower crustal xenoliths and megacrysts (Sutherland *et al.*, 1989). The Table Cape flow extends west towards Boat Harbour and was dated between 13–14 Ma (Sutherland & Wellman, 1986).

Inland, the extensive weathering with lateritic and red soil developments obscure the basalt relationships, apart from a few road cuts and landslip exposures. The Cassidys Creek zircon site, 1.75 km SW of Boat Harbour Post Office, yields fragments of several basalt types and only minor outcrops of flows. This may indicate a breccia/dyke source related to a small eruptive centre. The Cassidys Creek rocks range from highly undersaturated to near primary nephelinitic compositions to more highly evolved basanites and nepheline hawaiites and mugearites. Some rocks contain mantle assemblages in their xenolith suites, others contain only crustal xenoliths. Zircons were recovered directly from two members of the nepheline hawaiite-mugearite suite.

Basalt Sequence and Age Dating

Within the Cassidys Creek sequence, olivine melilite nephelinite and olivine nephelinite give the oldest ages (Late Oligocene 26.3–26.4±0.2 Ma ages; Sutherland & Wellman, 1986 and Table 1, Appendix). An evolved alkaline lava, with anorthoclase and zircon xenocrysts, yields a younger mid-Miocene age of 14.2±0.1 Ma (Table 1). The dated flow contains fresh phenocrysts, but the groundmass includes some alteration so that the K-Ar age may be slightly lower than the true age of extrusion. These rocks are capped on the north bank of Cassidys Creek by a distinct, blocky-jointed coarse basalt, which weathers into red soils. In petrography, this basalt resembles Table Cape teschenite dated at 13.3±0.2 Ma (Sutherland & Wellman, 1986) and yields no zircons from soils panned from its weathered top.

Zircons sampled from alluvial deposits below zircon-bearing basalts include prominent coloured crystals. These gave a fission track age of 13.9±0.7 Ma (Table 2, Appendix), supporting the mid-Miocene K-Ar age for the evolved lavas. Pale, rounded, small zircon grains, which contrast with the typical zircons, give lower uranium contents (30–281 ppm cf. 193–441 ppmU) and a younger fission track age of 9.5±0.6 Ma (Table 1). A similar age is recorded from basalt in northwest Tasmania (Baillie, 1986) and suggests such activity took place near Boat Harbour, although the source for these zircons is not yet identified.

The combined K-Ar and zircon fission track dating (Fig. 1; Tables 1, 2) indicates at least three eruptive episodes in the Cassidys Creek section.

— Late Oligocene nephelinitic activity (26–27 Ma)

— Mid-Miocene zircon-bearing evolved alkaline activity (14–15 Ma) and slightly evolved alkaline activity (13–14 Ma)

— Late Miocene zircon-bearing alkaline (?) activity (9–10 Ma)

Analytical Procedures

Representative analyses were made of mineral phases in the basaltic rocks, their xenocrysts and xenoliths. They are presented in Tables 3–10 (Appendix) and summarised in triangular diagrams for pyroxenes (Fig. 2a), olivines (Fig. 2b) and feldspars (Fig. 3). Analyses were made by electron microprobe and two different instruments

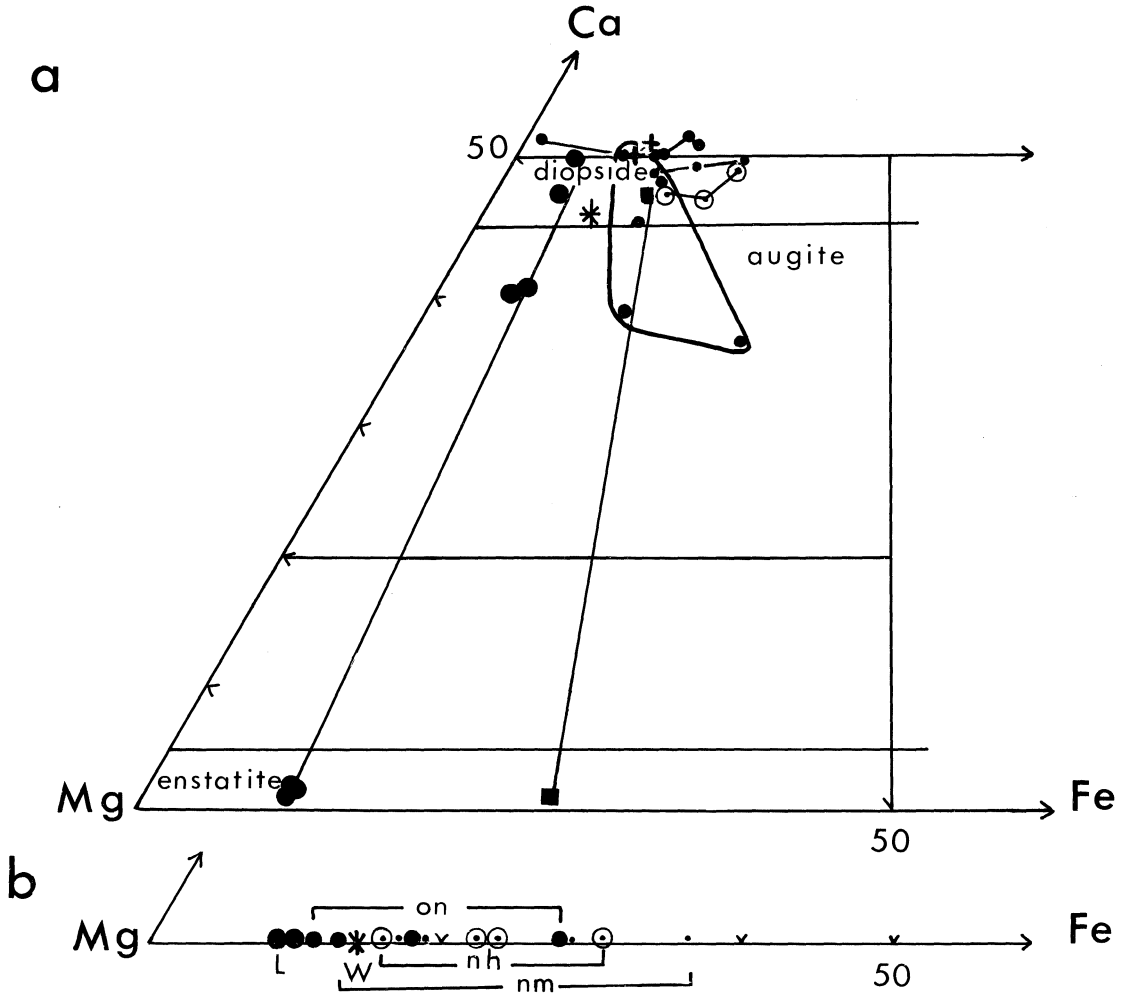

Fig. 2. a. Pyroxene compositions in Cassidys Creek host rocks, segregations and xenoliths plotted in an Mg-Ca-Fe diagram. Olivine melilite nephelinite (crosses), olivine nephelinite (solid dots, with those of segregations enclosed in a field), nepheline hawaiite (circled dots, with those of segregations joined by tie lines), nepheline hawaiite (small dots), lherzolite xenoliths and metasomatic replacements (solid large circles), wehrlite xenoliths (asterisk) and granulite xenoliths (solid squares). Two-pyroxene assemblages co-existing in xenoliths are joined by solid tie lines. Pyroxene nomenclature after Morimoto (1988). **b.** Olivine compositions Cassidys Creek lavas and xenoliths. Olivine nephelinites (on) solid circles, nephelinite hawaiites (nh) circled dots, nepheline mugearites (nm) small dots, lherzolite xenoliths (L) large dots, wehrlite xenolith (W) asterisk.

were used. Most analyses were obtained in a combined wave length/energy dispersive system at the Electron Microscope Unit, University of Sydney, with wave length spectrometers used to improve detection limits on key elements such as Na and K (D.F.H. analyst). Other analyses were made on an automated ETEC microprobe at Macquarie University, using natural standards, Bence-Albee matrix corrections and 15kV accelerating voltage (B.J.B. analyst). These methods yield precisions better than ±1% for elements present at above 10wt% as oxide, ±5% at 1–10wt% levels and ±10% at levels below 1wt%. Comparative analyses from the two instruments usually agree within ±2% for oxides over 5wt%, within ±8% for oxides between 1–4wt% and ±30% for oxides below 1wt%.

Bulk rock chemistry on the basalts was determined for major elements by X-ray fluorescence spectrometry, using fused borate button sample preparation, with Na determined by flame photometry and FeO determined by dissolution with HF in presence of ammonium metavanadate and titration against standardised ceric sulphate. These methods gave a precision around 0.6%. Trace elements were determined from pressed powder samples with boric acid bases, by X-ray fluorescence, using mass absorption data derived for major element analyses. Water and CO_2 determinations were made on most rocks, although some were made only as ignition loss.

The nomenclature of basalt types is based on the bulk chemistry given in Table 11 (Appendix) and follows the

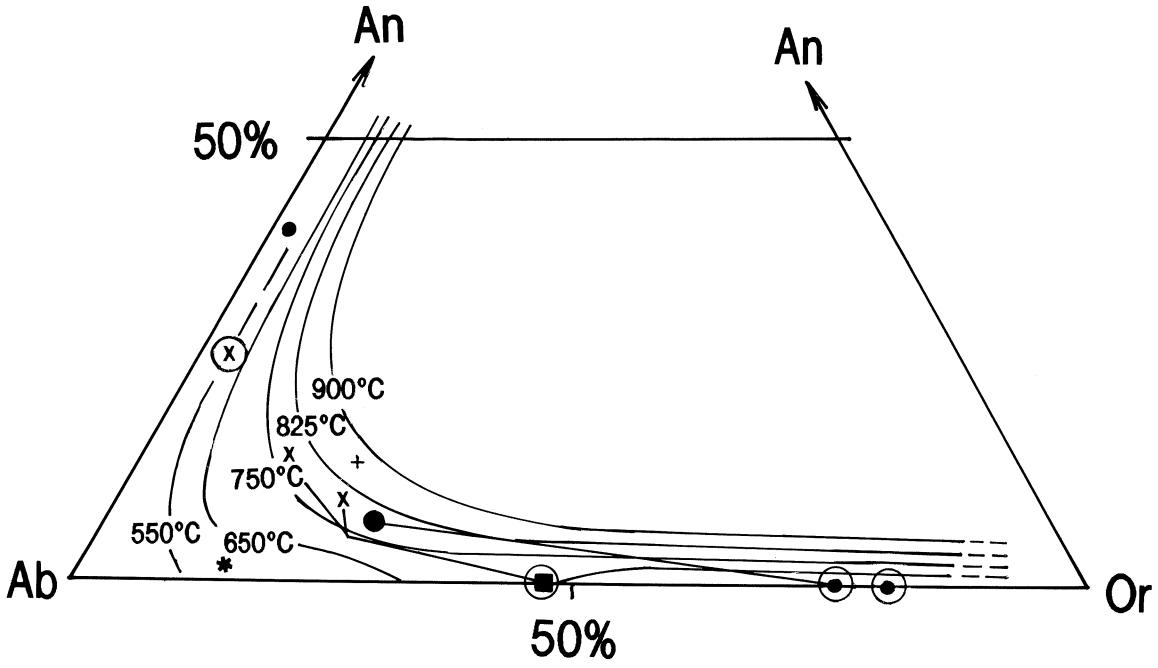

Fig. 3. Alkaline feldspar compositions (<50% An) for Cassidys Creek groundmass, segregation, xenolith replacement, xenolith and megacryst phases plotted in an Ab-Or-An diagram. Anorthoclase; nephelinite groundmass (solid circle), nepheline hawaiite segregation (inclined cross), nepheline mugearite (upright cross), megacryst (asterisk). Sanidine; nephelinite mariolite (solid centred circle), lherzolite replacement (solid square). K-oligoclase; anorthosite (circled cross), andesine-2pyroxene granulite (dot). Feldspars from related rocks are joined by solid lines. Temperature isotherms at 1000 bars come from the experimental work of Seck (1971), with equilibrium plagioclase-alkali feldspar compositions at 900°C and 500 bars connected by tie lines.

classification proposed for east Australian volcanic rocks by Johnson & Duggan (1989). Detailed petrographic descriptions of the basalts are given in Table 12 (Appendix).

Basalt Types

The rocks include olivine±melilite nephelinites, nepheline hawaiites and nepheline mugearites. The nephelinites and some mugearites contain mantle xenoliths along with crustal fragment suites, so represent magmas erupted from mantle depths. Other nepheline hawaiites and mugearites only contain crustal inclusions or no obvious inclusions. This does not mean unequivocal eruption from crustal chambers, as it may involve selective sampling within the magmatic plumbing systems.

Olivine melilite nephelinites (Analysis 1, Table 11 and Sutherland *et al.*, 1989) have near-primary Mg numbers (0.67–0.68). Microphenocrystic olivine, melilite and ulvospinel appear with groundmass clinopyroxene, ulvospinel and feldspathoids, which include sodalite (Table 12). Melilite end member compositions range between 60–65% akermanite, 34–36% soda-melilite and 0–5% gehlinite and the nepheline includes 25–28% of the potassic kalsilite end member (Ewart, 1989).

Olivine nephelinites (Analysis 2, Table 11) show a primary Mg#(0.69). Olivine phenocrysts and diopside microphenocrysts appear with groundmass olivine, clinopyroxene, ulvospinel, nepheline and alkali feldspar. A glomeroporphyrite texture in which clinopyroxene contains inclusions of olivine and ulvospinel suggests an early crystallisation for these minerals.

Late segregations in the groundmass become richer in nepheline and alkali feldspar, accompanied by more Fe-enriched olivine, diopside, ilmenite, amphibole and mica. Rare ovoid mariolitic cavities contain coarse growths of these minerals and the presence of sodalite, hydrous phases and euhedral crystals projecting into the cavity suggest growth in volatile-rich, chlorine-bearing fluids. There are some overlaps in the crystallisation sequence of these late-growth minerals (Table 12), but the general paragenetic sequence is olivine, then diopside, amphibole, sodian augite, sodalite, nepheline, ulvospinel, sanidine, phlogopite and carbonate. In some variants clinopyroxenes lack olivine inclusions and contain resorbed cores and, in others, apatite is more abundant and mica is rare. These may represent more evolved residues.

Nepheline hawaiites (Analyses 3, 6–7, Table 11) are moderately evolved rocks (Mg# 0.56–0.61). They range from aphyric to more porphyritic types.

Aphyric nepheline hawaiite (Analysis 3) is rich in nepheline, accompanied by olivine clinopyroxene, alkali feldspar and ulvospinel. Microporphyritic nepheline hawaiites (Analyses 6–7) show similar Mg#s (0.56–0.58) but contain anorthoclase and zircon xenocrysts and microphenocrysts of olivine and diopside. The groundmass includes plagioclase, nepheline, alkali-feldspar and ulvospinel (Table 7). Mariolitic cavities are infilled by diopside, anorthoclase, nepheline and ulvospinel and amygdales by zeolites.

The aphyric nepheline hawaiite (Mg# 0.58) and Table Cape-nepheline hawaiites (Mg# 0.61) are lower in SiO_2 but higher in MgO and CaO than the porphyritic types which are enriched in alkalis (cf. Analyses 3 & 4 with Analyses 6–7).

Nepheline mugearites (Analyses 5, 8–9) show Mg#s (0.57–0.60) similar to the nepheline hawaiites, but normative An% is lower (<30%) reflecting more alkaline compositions. They also carry anorthoclase and zircon xenocrysts and typically contain microphenocrysts of olivine and clinopyroxene in a groundmass of olivine, clinopyroxene, ulvospinel, nepheline, alkali feldspar and yellow glass (Table 6). Some show abundant apatite inclusions in the late alkali feldspar and thin feldspathic segregation veins.

Xenocrysts

Most xenocrysts are derived from the typical xenoliths suites found in the rocks. However, a few distinctive xenocrysts are present.

Anorthoclase is prominent in several evolved lavas, both in the mantle and crustal xenolith-bearing types. Crystals range up to a few centimetres across and show resorbed margins. Restricted core compositions (Table 6) fall in the sodian anorthoclase range (Ab_{82-84} Or_{13-15} An_{3-4}) and are more sodian than groundmass and late segregation anorthoclase within the host rocks.

Zircon includes hafnium and thorium-bearing examples (Hf 1.1wt% and Th 0.2wt%; Hollis *et al.*, 1986) and uranium may exceed 440 ppm (Table 1). A feature of the zircon is rare earth patterns that lack europium depletion (Sutherland, 1996). This does not support its crystallisation from evolved basaltic liquids, so the zircons are true xenocrysts in relation to their hosts. More detailed investigations of the zircons will be presented elsewhere.

Olivine in one nepheline mugearite, includes olivine that is too magnesian (Fo_{90-91}) to relate to the host (olivine phenocrysts Fo_{81}) or to disaggregated spinel wehrlites (olivine Fo_{85}) in the rock (Table 9). The olivine is simply twinned and thinly rimmed by olivine crystallised from the host. The Ca content (0.1wt%) may indicate a high temperature basaltic origin rather than disintegration of mantle lherzolite, in which olivines show CaO under 0.1wt% (Ewart, 1989). Enstatite (En_{89-90}) xenocrysts in the rock in contrast shows compositions and reaction rims typical of disaggregated mantle lherzolites.

Xenoliths

Mantle xenoliths are dominated by spinel lherzolites, but one nepheline mugearite also carries rare wehrlite besides lherzolites. Crustal xenoliths include common quartzitic metasediments, and rare granulites and anorthosites.

Spinel lherzolites (Table 8) contain anhedral olivine (Fo_{89-91}) up to 5mm across, intergrown in metamorphic textures with diopside (Wo_{37-38} En_{57-58} Fs_{5-3}), enstatite (En_{88-89} Fs_{9-10} Wo_{1-2}) and interstitial chromian spinel (Sp_{78-84} Cm_{10-17}). Xenoliths range from pristine to partially altered. These assemblages give re-equilibration temperatures around 900–920°C based on Cr-Al-orthopyroxene thermometry (Witt-Eicksen & Seck, 1991). This correlates with mantle pressures between 8–9kb (around 30 km depth) when projected on to the nearby Table Cape Tertiary geotherm (Sutherland *et al.*, 1989).

Infiltration and reaction occurs along grain boundaries giving incipient alteration of pyroxenes and replacing chromian spinel by rims of opaque oxide. Greater reaction with pyroxenes creates embayments and invasions of glassy melt. This melt has a hydrous, potassic intermediate-siliceous composition (Table 8), with normative compositions akin to that of magnesian "minette" (cf. Rock, 1991). This suggests introduction of K-rich fluids into the fresh lherzolite, which shows no potassic phases. Glasses are recorded from incongruent melting in lherzolite (Francis, 1987), but their compositions are higher in Si, Al, Ca, Na and lower in K and volatiles than the Cassidys Creek glass. The latter resembles glasses linked to metasomatic infiltrations of lherzolites under both mantle and crustal pressures (Francis, 1991; Hornig & Wörner, 1991; Draper, 1992). It best fits reaction of lherzolite with alkaline K-rich and volatile-rich fluids represented by the sanidine, phlogopite and carbonate crystallisation in late segregations in the host basalt.

Under extreme reaction and melting, the lherzolite grains become completely replaced by a finer grained mineral assemblage (Table 8). Reaction with chromian spinel mainly replaces Al by Si, probably reflecting incipient spinel-feldspar reaction. Melt recrystallises into olivine (Fo_{89}) sodian and chromian augite (Wo_{34} En_{61} Fs_5 containing up to 6% acmite and 2% jadeite end members), soda sanidine (Ab_{52-54} Or_{46-48}) and minor opaque oxide.

Spinel wehrlite (Table 8) contains coarse (up to 6mm) aluminian, sodian diopside (Wo_{36}, En_{60} Fs_4) containing 13% of the jadeite end member. It is intergrown with olivine (Fo_{85}) and pleonaste (Sp_{79-80} Hc_{15} Mt_{4-5}) in grains

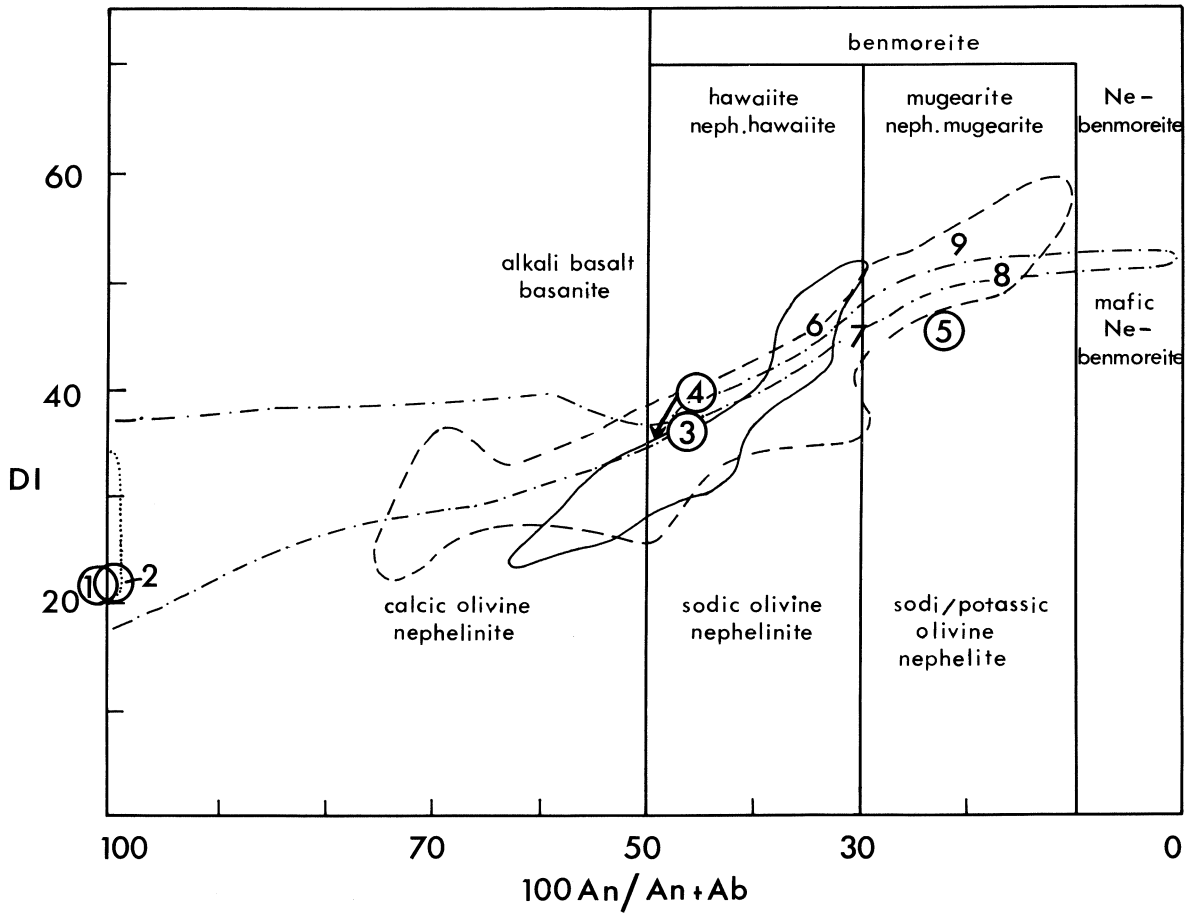

Fig. 4. Differentiation Index (D.I.) against 100 An/An+Ab (Analyses 1–9), Cassidys Creek-Table Cape volcanic rocks related to Tasmanian basaltic fields. Lherzolite-bearing rocks are circled. Tasmanian olivine melilite nephelinite (dotted line), olivine nephelinite lineage (dot-dashed line), basanite lineage (dashed line), alkali basalt lineage (solid line).

up to 4.5 mm across. The texture suggest a cumulate assemblage. Comparisons of the mineral compositions with those from mantle xenocrysts and the phenocrysts in the host nepheline mugearite (Table 8) supports a high pressure mantle origin from fractionating basanitic magma (Sutherland *et al.*, 1984; Griffin *et al.*, 1984).

Quartzitic metasediments show fragments rimmed by or completely fused into brown glass, with incipient developments of new minerals.

Granulites include two-pyroxene assemblages (Table 10) in which enstatite (En_{72-73} Fs_{27-28} Wo_{0-1}), and diopside (Wo_{42} En_{46-47} Fs_{11-12}) show irregular triple point intergrowths with abundant andesine (Ab_{56-61} An_{36-39} Or_{2-7}). Re-equilibration temperatures (Wells, 1977 and Wood & Banno, 1973 thermometry) range between 860–880°C and when projected onto the Tasmanian Tertiary geotherm (Sutherland *et al.*, 1989) suggest re-equilibration pressures around 7kb, equivalent to about 25km depth.

Anorthosites (Table 10) contain andesian zoned from less sodian cores (Ab_{70-71} An_{26-27} Or_{3-4}) to more sodian rims (Ab_{71-75} An_{20-25} Or_{3-4}). Some grains show reaction coronas around quartz, where infiltrating fluids melted boundaries into siliceous glass containing indeterminate iron oxides, alumino-silicates and skeletal sanidine (Ab_{49-51} On_{49-51}). The texture suggest feldspar accumulation around quartz grains by magmatic reaction rather than a granulitic origin.

Geochemistry of Basalts

General features. The sequence (Analyses 1–9, Table 11) is consistently ne-normative and sodic with only minor variations in Na_2O/Na_2O+K_2O ratios(0.68–0.78) with changes in Differentiation Index (D.I. 20–55), normative An/An+Ab (0.17–1.00), $Mg/Mg+Fe^{2+}$ (0.56–0.70) and $Al_2O_3/CaO+Na_2O+K_2O$ (0.44–1.03). However, there is a clear separation between the primary nephelinites and more evolved alkali basalts in D.I. versus An/An+Ab plots (Fig. 4). In normative olivine-

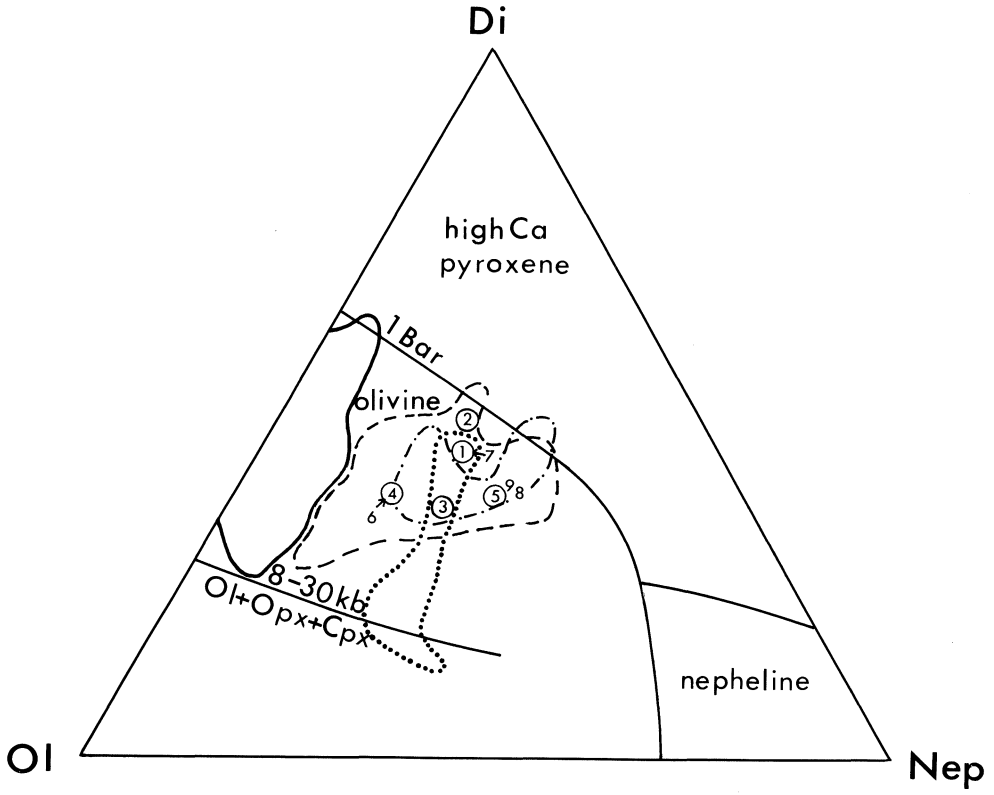

Fig. 5. Normative olivine (Ol)-nepheline (Neph)-diopside (Di) diagram showing plots of Cassidys Creek volcanic rocks (Analyses 1–9) relative to Tasmanian olivine melilitite, olivine nephelinite, basanite and alkali basalt lineages (fields as for Fig. 4). The cotectic experimental 1 bar and 8–30kb lines are after Sack *et al.* (1987).

diopside-nepheline diagrams, the primary nephelinites tend to higher D.I. values, but otherwise the field forms a relatively coherent group (Fig. 5). There is little separation between mantle and crustal xenolith bearing rocks in relation to the 1 and 8–30kb (ol+opx+cpx) cotectic projections (Sack *et al.*, 1987). This suggest magmas evolved at deeper crust/upper mantle levels, without extreme shallow crust modification.

Minor and trace element features. Among the minor elements Ti and K show contrasting trends. Ti decreases with evolution i.e. TiO_2 2.8–3.3% for nephelinites, 2.3–2.5% for nepheline hawaiites and 1.6–1.8% for nepheline mugearites. K increases with more evolved character, i.e. K_2O 1.1–1.3% for nephelinites, 1.9–2.1% for mantle xenolith-bearing nepheline hawaiites and 2.1–2.4% for nepheline hawaiites and nepheline mugearites. These trends no doubt involve differences in sources and melting for the magmas, but fractionation of phases in the evolved magmas probably played a part.

Crystallisation of phases, such as those in the spinel wehrlite cumulates dominated by titanian and sodian calcic clinopyroxene, would diminish TiO_2 and CaO and augment K_2O, as observed in the evolved rocks. Distinctly higher P is present in the more undersaturated rocks i.e. P_2O_5 1.2–1.6% below 43wt% SiO_2 and P_2O_5 0.8–0.9% in rocks above 43wt% SiO_2. No apatite fractionation is obvious in the sequence, so this may reflect a source melting characteristic.

Compatible trace elements (Ni, Cr, V, Co, Sc) show depletion with decreasing Mg# (Fig. 6) typifying fractionation involving magnesian minerals. However, there is little increase in incompatible elements such as Zr expected in typical fractionation (Fig. 7). The Zr contents show no significant variation with change in Mg# or D.I. (Fig. 8). Zr and Nb show positive correlation, but the range in Zr contents and Zr/Nb ratios differ between the nephelinites (Zr 370–452 ppm, Zr/Nb 3.7–3.9) and evolved basalts (Zr 201–430 ppm, Zr/Nb 4–5). This reinforces the separate origin of these rocks shown by age dating.

Available compatible trace elements, normalised to primitive mantle values, are compared in Fig. 9. The nephelinites show the greatest incompatible enrichments except for K and Sr in some instances. Most evolved basalts are characterised by Rb, Ba and Nd depletions, expect for some nepheline mugearites with high Ba. Remaining trace elements show little coherent change across the suites, except for Th and Pb which peak in the olivine melilite nephelinite and Cu which decreases relative to Zn in the evolved basalts.

At least three trace element groups are found in the Cassidys Creek suites.

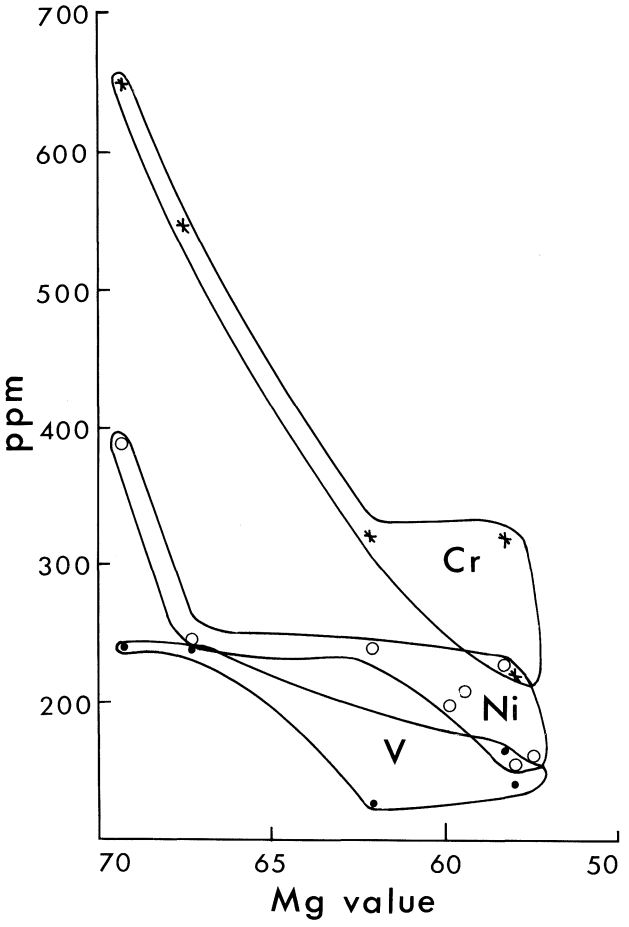

Fig. 6. Cassidys Creek compatible trace elements values (ppm), plotted against Mg value (Table Cape excluded). Chromium (stars), nickel (open dots), vanadium (dots). Analyses 1–3, 5–9.

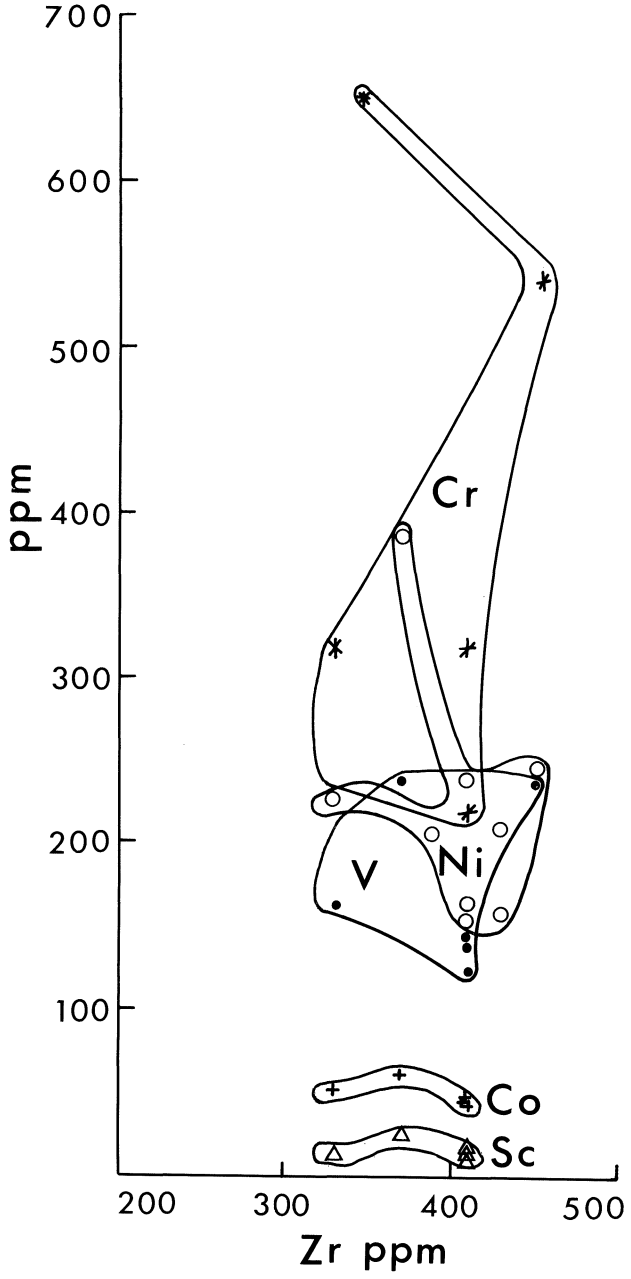

Fig. 7. Cassidys Creek compatible trace element values (ppm), plotted against Zr (ppm). Cr, Ni and V fields as for Fig. 6, with Co (crosses) and Sc (triangles).

1. Nephelinites with low Zr/Nb (3.7–3.9), Sr/Ba (2.5–4.2) and Rb/Nb (0.19–0.25) and high Ba/Rb (10.4–22.4);
2. Nepheline hawaiites and mugearites with higher Zr/Nb(4.0–5.0), Sr/Ba (13.7–22.5) and Rb/Nb (0.21–0.33);
3. Nepheline hawaiite and mugearites with significantly lower Sr/Ba (4.85–5.5) and higher Ba/Rb (11.8–15.0) than in the other evolved rocks.

In general, Zr/Nb ratios increase with degree of partial melting of mantle sources that generates the olivine melilitite-tholeiite petrogenetic spectrum (Frey *et al.*, 1978). This can be represented by plotting Zr/Nb against (ne+lc) for the undersaturated members (Fig. 10), after Green (1992). The higher Zr/Nb for the evolved lavas is consistent with a higher degree of source melting than for the nephelinites, and implies a basanitic parent magma may involved.

Origin and Evolution of the Magmas

The high Mg# and low Zr/Nb for the nephelinites typify primary low degree partial melts that retain inputs from their source conditions, whereas the lower Mg# and higher Zr/Nb for the evolved lavas typify modified magmas in which source inputs become masked.

Primary Sources for nephelinites. The co-existence of both melilite-bearing and normal nephelinites at the one site, has relevance to likely source conditions. Such

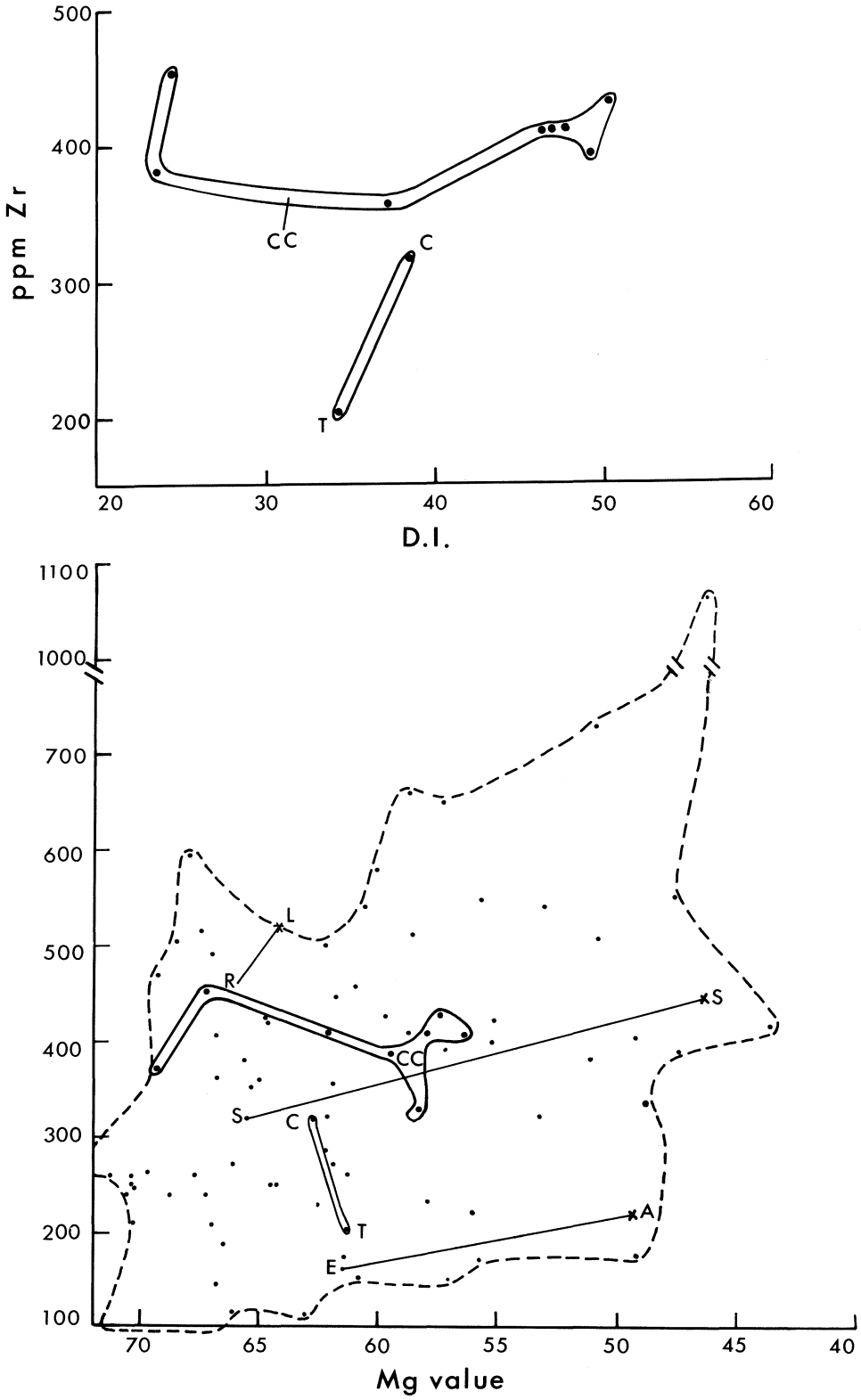

Fig. 8. **a** (above): Zr trace element contents plotted against D.I.: Cassidys Creek field CC, Table Cape field TC. Analyses 1–9 and F.L. Sutherland, unpublished data. **b** (below): Zr (ppm) values plotted against Mg values for Cassidys Creek (CC) and Table Cape (TC) fields, in relation to values plotted for other Tasmanian basalts; data from Frey *et al.* (1978), Everard (1984, 1989) and Sutherland (1984, 1985, 1989a and unpublished). Host and late-stage pegmatoid trends are joined by tie lines for Round Lagoon olivine nephelinite (RL), South Scottsdale olivine nephelinite (SS) and East Arm basanite (EA). The Sandy Bay mafic nepheline benmoreite plot is off scale and shown as a discontinuous value.

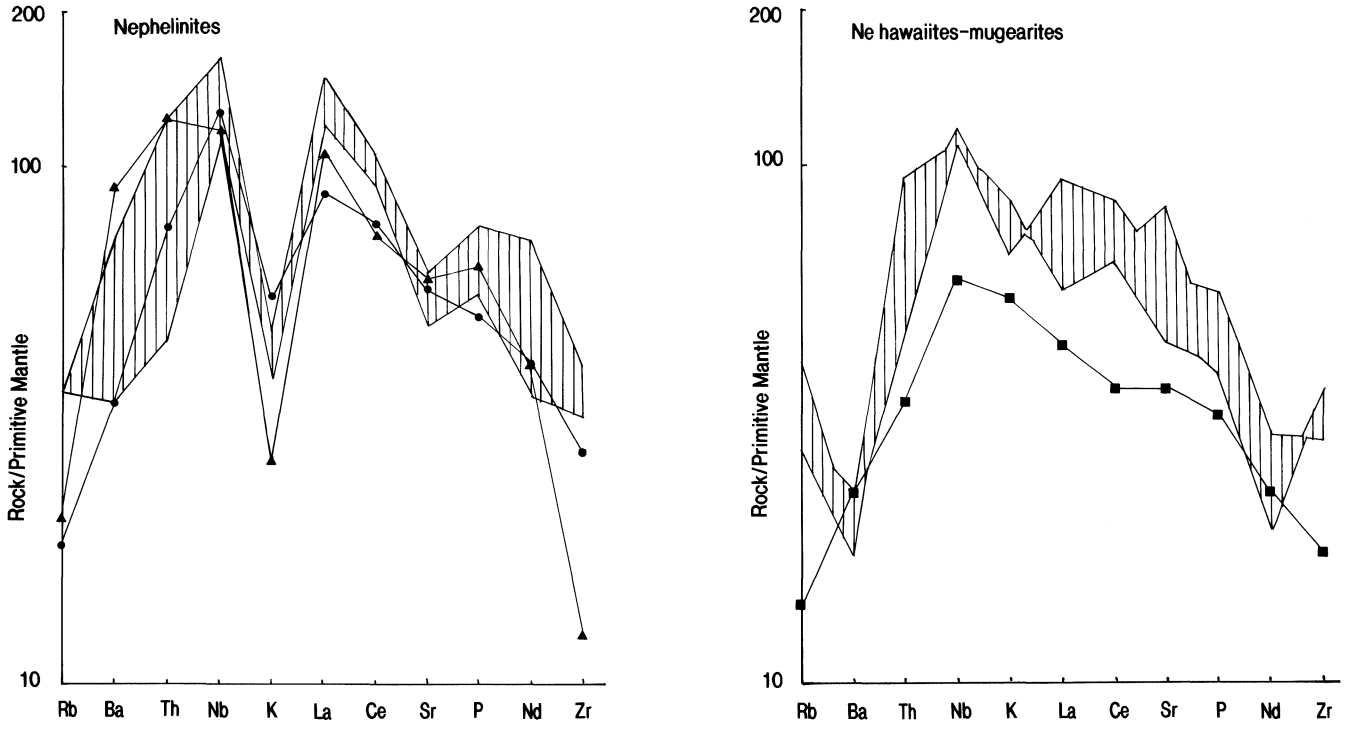

Fig. 9. Comparative incompatible minor and trace element patterns envelopes (filled sections) for Cassidys Creek-Table Cape rocks, with nephelinites (left) and ne hawaiites-mugearites (right). Elemental abundances are normalised to primitive mantle values after Sun & McDonough (1989). Cassidys Creek nephelinites are contrasted with low Rb nephelinites from NE Tasmania (joined solid dots, data from Frey *et al.*, 1978) and Barrington volcanic province, New South Wales (joined triangles, data from O'Reilly & Zhang, 1995). Cassidys Creek evolved rocks are contrasted with low Rb nepheline hawaiite from Table Cape (joined squares, data from Table 11). The Ba enriched Cassidys Creek ne mugearite (Analyses 8–9) are not plotted due to restricted incompatible element data.

rocks in Tasmania were investigated geochemically and experimentally (Brey & Green, 1977; Frey *et al.*, 1978; Adam, 1990). The earlier work favoured low degrees of partial melting (4–7%) of garnet lherzolite mantle at 1150–1250°C and 27–30kb, with melilitic magmas generated under high CO_2/H_2O ratios. Up to 14wt% volatiles were needed to achieve equilibrium with a garnet lherzolite source. Later experimental work (Adam, 1990) suggests that such magmas can form under lower volatile contents (<7wt%), with pressures controlling the magma types rather than CO_2/H_2O ratios. Thus, the Cassidys Creek melilite nephelinite could indicate deeper source levels than for the nephelinite, without invoking significant H_2O/CO_2 variability in the sources.

The relatively high TiO_2/Y (970–1105) and Zr/Y (10.5–11.5) key ratios for the nephelinites indicate some garnet remained in the source after melting, while CaO/Na_2O ratios (3.1–3.8) suggest significant diopside/jadeite melting or suppression of diopsidic activity through Ca-carbonate ion bonding (Frey *et al.*, 1978).

Metasomatised sources for nephelinites. The high P_2O_5, LREE and Nb in the nephelinites are compatible with 4–8% partial melting of an enriched garnet lherzolite source (Brown & McClenaghan, 1982). This, combined with the high Sr, Ba, Rb, Th, La, Ce and Nd, suggests melting of non-refractory phases, such as amphibole, mica and apatite (O'Reilly & Griffin, 1984; O'Reilly *et al.*, 1991). Wall rock reactions between melts and metasomatised mantle above the source may also alter final trace element contents, but imprints of the main source contributions probably survive (O'Reilly *et al.*, 1991). Metasomatic amphibole and mica also increases Ti and Fe relative to Mg (Wilkinson & LeMaitre, 1987). Greater contribution of such metasomatised phases in the melilite nephelinite source can account for its higher Ti/Mg and Fe/Mg relative to the olivine nephelinite. Low degree melting produced in equilibrium with such Fe enriched sources would also crystallise less magnesian olivines on the liquidus, as suggested by comparative phenocryst compositions in the melilite nephelinite (Fo_{84}) and nephelinite (Fo_{88}). The Na/K ratios (0.74–0.78) of the nephelinites suggest amphibole dominated over mica in their contributions to the melt.

Crystallisation within nephelinites. Low pressure crystallisation trends in the nephelinite melts after eruption are given by changes in mineral compositions phases in phenocrysts, groundmass grain and mariolitic infillings (Tables 4, 7 and Figs 11, 12). Olivine becomes less magnesian (Fo_{84-88} to Fo_{72}). Early pyroxenes show complex compositions, due to Al, Ti and Na substitutions

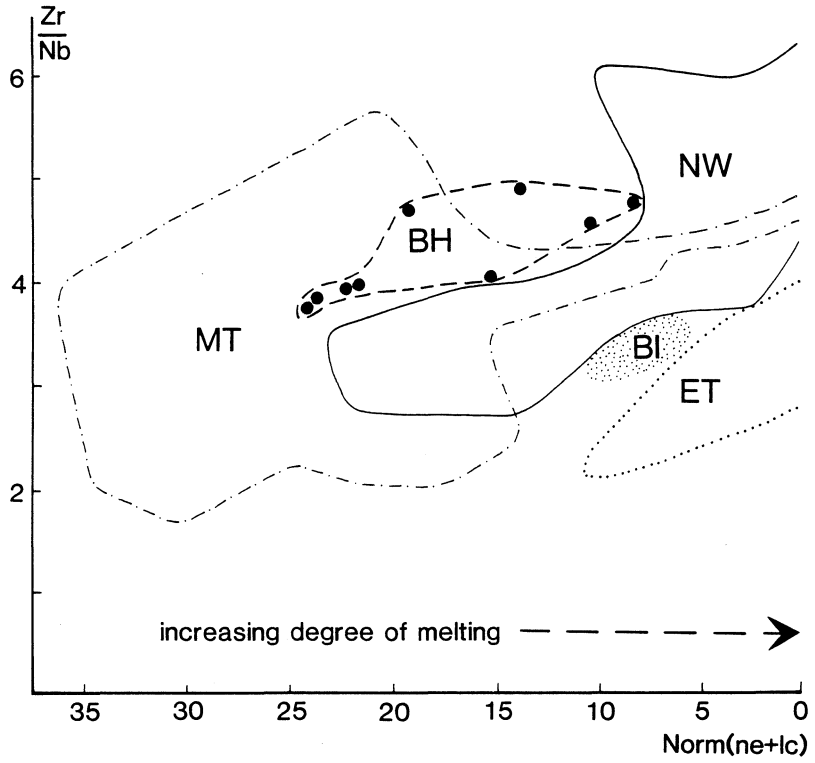

Fig. 10. Boat Harbour Zr/Nb ratios (solid dots) plotted against normative ne + lc. BH Boat Harbour alkaline field (dashed lines), MT Mid-Tasmanian alkaline field, (dot-dashed lines), NW North West Tasmanian alkali basalt field (solid line), ET East Tasmania alkali basalt field (dotted line). BI, Balleny Islands (Sabrina Island) field (stippled area), Data from this paper; Frey *et al.* (1978); Everard (1984, 1989); Sutherland (1989a,b); Sutherland *et al.* (1989); Green (1992) and F.L. Sutherland, unpublished.

in the structure (Wo_{39} En_{35-36} Fs_{0-1} Cfs_{9-10} Cta_{4-5} Jad_{11-12}), but late pyroxenes become poorer in Ca and Mg components and richer in Na and Fe end members (Wo_{35} En_{29-30} Fs_{5-6} Jad_{2-3} Acm_{27}). Nepheline becomes more potassian (Ne_{84} Ks_{19} Q_6 to Ne_{79} Ks_{17} Q_4) and alkali feldspar more potassian and barian (Ab_{66} Or_{27} An_{57} to Ab_{24} Or_{71} Cn_5). These trends (Fig. 11) resemble those for low pressure fractional crystallisation of nephelinites towards malignitic compositions (Wilkinson, 1977). Hydrous and halogen-bearing minerals (amphibole, mica, sodalite) and carbonates and zeolites appear in late crystallisation and indicate an alkaline volatile-rich end-stage.

Ba increases in the late alkali feldspars, consistent with crystallisation at lower temperatures and pressures (Guo & Green, 1989) and the Ba/K and Al/Si ratios in the alkali feldspars suggest crystallisation under 950°C. The co-existing sanidine and anorthoclase compositions in the late segregations suggest final crystallisation below 825°C (Seck, 1971; Fig. 3).

Origin of the evolved members. No primary parental basanites or basalts for evolving nepheline hawaiites and mugearites (Mg# 0.56–0.62) were identified in the sequence. The nepheline hawaiite with lowest SiO_2 (43wt%) still shows a relatively reduced Mg# (0.58) compared to a primary parent.

Potential fractionation steps for the evolved rocks were evaluated using the MAGFRAC program (Morris, 1984). This matches compositions of less evolved and more evolved members of a rock series using constituent minerals in the more evolved rock. Proportions of fractionating phases are calculated and the feasibility of the process is tested by a least squares residual method. No satisfactory solutions were found for deriving any member from less evolved compositions (including the Table Cape nepheline hawaiite). Contamination of compositions through incorporation of xenoliths (lherzolite, quartzite) and secondary mineral fillings may be involved, but was minimised in the analysed pieces and cannot explain high residuals in some elements. In addition, the rocks lack the high SiO_2, low Nb/Y and negative Nb anomalies found in strong crustal contamination (Campbell & Griffiths, 1992). The main problems lie in high Na, K, Ti, Fe and Al residuals left after attempted fractionation. These remained even after adding a sodian anorthoclase megacryst composition and using a theoretical ilmenite composition instead of the observed ulvospinel. This either indicates fractionation of different phases at depth (e.g., amphibole and mica) now unrepresented in the lavas except as minor late-stage phases, or evolution of members from varied batches of parental magmas. The first option is not

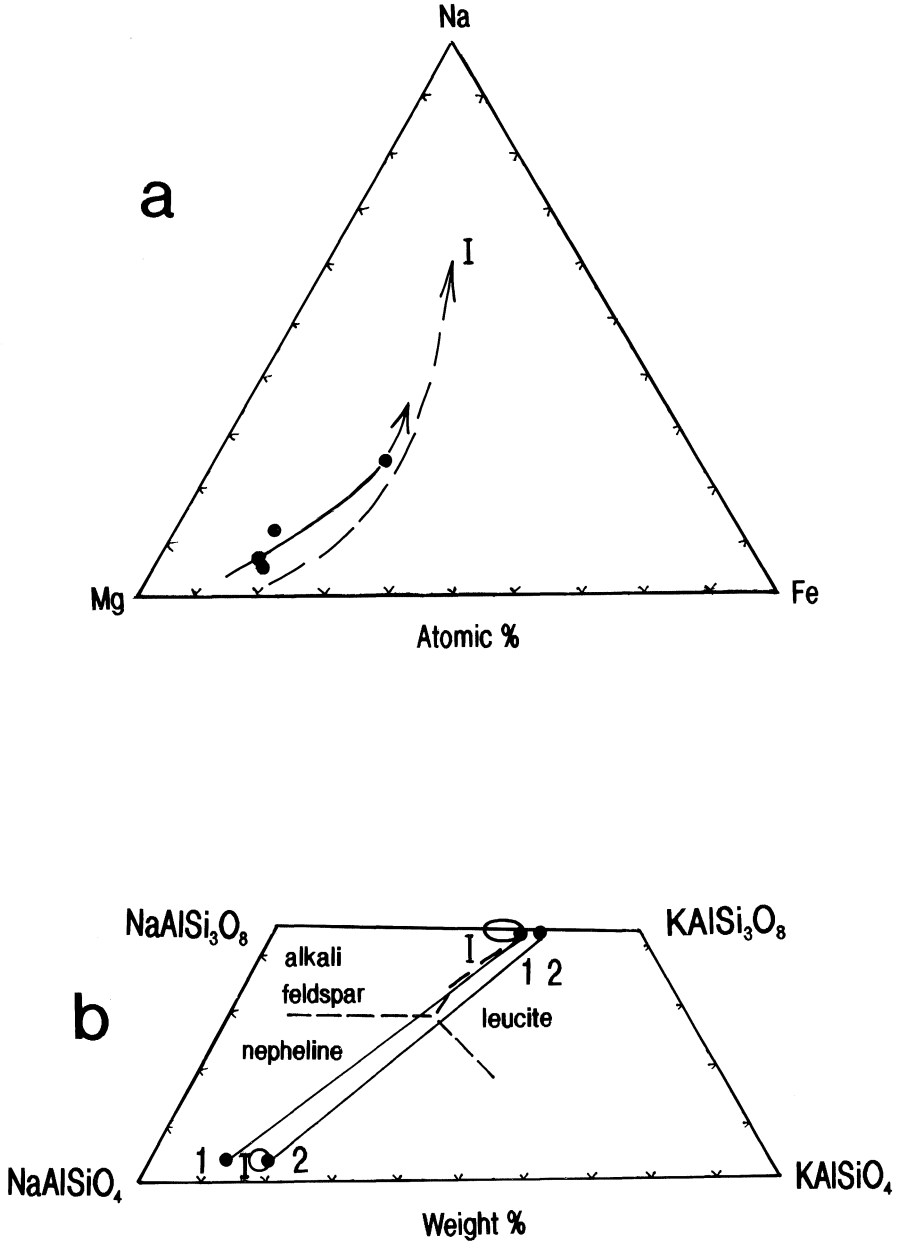

Fig. 11. Comparative pyroxene, nepheline and alkali feldspar compositions from Cassidys Creek and Inverell olivine nephelinite and associated late mariolitic segregations. **a**. Mg-Fe-Na diagram showing Cassidys Creek plots (dots) and trend (solid arrow) compared to Inverell trend (I, dashed arrow, from Wilkinson, 1977). **b**. Undersaturated quadrilateral residua system for nepheline and alkali feldspars showing plots (dots) of Cassidys Creek co-existing nepheline and alkali feldspar (joined by tie lines), with 1 olivine nephelinite groundmass, 2 late segregation. Comparative Inverell, NSW, compositions are shown by enclosed circles (I) and the nepheline-alkali feldspar-leucite boundary curves at P H_2O = 1000 bars are designated by heavy dashed boundaries, after Wilkinson (1977).

readily testable, but fractionation involving Ti amphibole to reduce Na, Ti and Fe (Green *et al.*, 1974) would increase SiO_2 and K_2O over the typical Cassidys Creek values. Similarly Ti-mica fractionation would exacerbate SiO_2 and K_2O mismatches. The presence of high pressure cumulate wehrlite in a mantle-derived nepheline mugearite favours fractionation of melts through crystallisation of phases observed as phenocrysts in these rocks.

A potential parental trend can be estimated from an evolved composition (Analysis 5, Table 11) through addition of the wehrlite phases (Table 9), in their approximate modal proportions (Cpx_5 Spl_3 Ol_2). Even if the cumulate is not directly related to the host, its

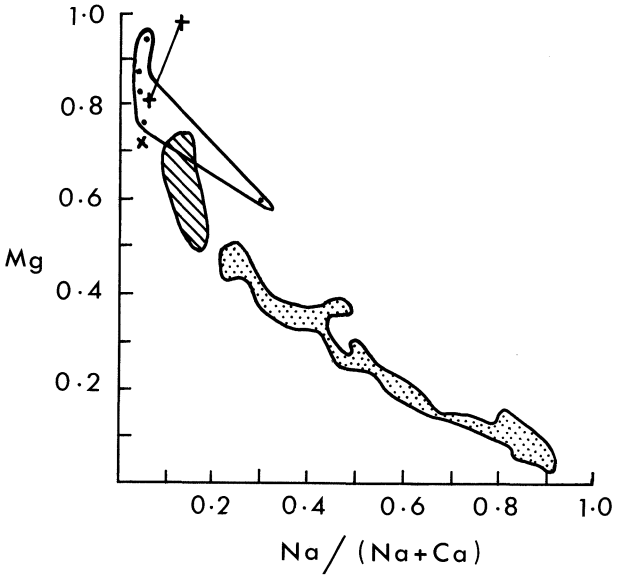

Fig. 12. Mg and Na/Na+Ca plots for Cassidys Creek late-stage pyroxenes, compared to evolved pyroxenes values from Tenerife Canary Island magma chamber (Wolff, 1987). Dots enclosed in open field: Cassidys Creek olivine nephelinite. Inclined cross: Cassidys Creek nepheline hawaiite. Tied crosses: Cassidys Creek melt reaction vein in lherzolite. Hatched field: Tenerife phonolites. Stippled field: Tenerife sodalite-nepheline syenites.

presence indicates potential for such fractionation. A 10% addition of wehrlite mineralogy produces a near primitive nepheline hawaiite magma (Mg# 0.66, an/an+ab 44%, ne 19%). A 15% addition produces a primary basanite magma (Mg# 0.68, an/an+ab 52%, ne 19%). More primitive compositions are achieved by adding observed megacryst olivine (Mg_{90}), as an early liquidus phase. The estimated primary basanite remains strongly sodic (Na_2O/Na_2O+K_2O 0.74) in this fractionation scheme. Such a primitive basanite (ne hawaiite) from Oatlands, Tasmania (Mg# 0.68, an/an+ab 46%, ne 16%) was investigated experimentally by Adam (1990). The near-liquidus phase relationships were consistent with melting of garnet lherzolite mantle at 26kb and 1200°C for a magma containing 2wt% CO_2 and 4.5wt% H_2O.

Further evolution. The anorthosites with quartz nucleii suggest some high-level feldspar crystallisation within the evolved lavas. However, lack of feldspar phenocrysts in the rocks and the negative correlations achieved in using anorthoclase megacrysts compositions in the MAGFRAC calculations for evolving these rocks limits feldspar controls. This is reinforced by positive Ba and Ca correlations, which are incompatible with plagioclase control, and by enrichment in Ba over Rb in the highest Ba-value evolved rocks, which does not accord with alkali feldspar control.

The anorthoclase megacrysts may represent more felsic magma at depth, being more sodian than anorthoclase crystallising in the hosts (Ab_{81} Or_{15} An_4 cf Ab_{75} Or_{21} An_4). The negligible Ba (<0.2wt% BaO) in the megacryst anorthoclase is consistent with crystallisation at higher temperatures or pressures relative to late anorthoclase-sanidine crystallisation in the lavas, which took place below 825°C (Seck, 1971; Fig. 3). In considering Ba portioning in anorthoclase megacrysts in basalts, Guo *et al.* (1992) favoured their growth from melts of benmoreite compositions. These points and lack of alkali feldspar fractionation in trace element patterns of Cassidys Creek evolved lavas, suggests megacryst anorthoclase crystallised from a sodic benmoreite melt formed separately to the surface lavas. If the accompanying zircon megacrysts were also derived from these melts, then absence of Eu depletion in the zircon rare earth patterns further indicates they are not fractionated from the surface magmas.

Pyroxenes in late segregations, cavities and reaction veins in lherzolite xenoliths (Fig. 12) are compared with those evolving in highly differentiated undersaturated alkaline magma chambers (Tenerife, Canary Islands; Wolff, 1987). The high Mg and low Na/Na+Ca of Cassidys Creek pyroxenes suggest limited evolution. This probably also applies to underlying magmatic processes, as pyroxene phenocrysts in Cassidys Creek lavas are not significantly different in Mg/Na+Ca ratios to the late pyroxenes.

Cassidys Creek/Tasmanian Comparisons

Relationships of the Cassidys Creek sequence to other Tasmanian Tertiary volcanic rocks are compared in Figs 4, 5, 8 and 10.

Alkaline relationships. The Cassidys Creek sodic sequence differs from most Tasmanian alkaline lineages, that include K-rich rocks (Sutherland *et al.*, 1989), in its consistent sodic signature (Table 11). The more evolved rocks are the most soda-rich recorded in Tasmania. This sodic character extends to the prominent sodian anorthoclase megacrysts, that elsewhere are relatively rare in Tasmanian basalts. It may represent a local source signature, as it does not extend beyond Table Cape. There, basalt pyroclastics contain K-rich olivine nephelinite, although the succeeding nepheline hawaiite flow has similar Na/K ratio to Cassidys Creek rocks. Despite its distinctive Na/K ratios the Cassidys Creek sequence generally falls within Tasmanian lineages for such rocks (Fig. 4).

The Cassidys Creek nephelinites differ from some Tasmanian nephelinites (e.g., Scottsdale) in their incompatible element patterns, particularly in their relative K/Rb (Fig. 9).

Zirconium relationships. Cassidys Creek and Table Cape evolved rocks differ from most Tasmanian evolved sequences in showing negative to only minor positive correlations of Zr with increasing D.I. and Mg# (Fig. 8). The most evolved Cassidys Creek rocks are poorer in Zr (up to 430 ppm) than are similarly evolved rocks elsewhere in Tasmania (up to 660 ppm). Zircon megacrysts found in these relatively low Zr evolved

rocks are not readily equated with such Zr levels, as the magmas are insufficiently evolved to fractionate zircon to initiate such Zr depletions and the zircon REE lack typical fractionation patterns. The low Zr in these zircon-bearing rocks indicates little significant contamination has resulted through zircon resorption.

The Zr/Nb ratios of Cassidys Creek rocks (3.7–5.0) in relation to increasing feldspathoidal (ne +lc) content shows a restricted trend relative to the mid-Tasmanian alkaline association (Fig. 10). Their field extends away from the alkaline associations and falls outside the alkali basalt-tholeiitic basalt association in NW Tasmania. It is well removed from east Tasmanian alkali basaltic fields. This separate Zr/Nb trend for the evolved Cassidys Creek rocks reflects their unusual Zr content relative to similar Tasmanian rocks, with Zr and Nb reaching comparable levels in both primary and evolved rocks (Fig. 9).

Isotopic relationships. Limited strontium, neodymium and lead isotopic data on Cassidys Creek melilite nephelinite and Table Cape nepheline hawaiite (Ewart *et al.*, 1988) shows low radiogenic $^{87}Sr/^{86}Sr$ values (0.70294–0.70309±4) and relatively high $^{143}Nd/^{144}Nd$ (0.51292±13) and $^{206}Pb/^{204}Pb$ (19.141–19.656). Such isotopic values typify Tasmanian alkaline rocks and differ from most east Australian values (McDonough *et al.*, 1985; Ewart & Menzies, 1989). They reflect a HIMU (high U/Pb) mantle component mixed with a Mid-Ocean Ridge Basalt (MORB) component (Ewart *et al.*, 1988; Sun *et al.*, 1989; Lanyon *et al.*, 1993).

The Cassidys Creek nephelinites differ from some low $^{87}Sr/^{86}Sr$ Tasmanian nephelinites (Scottsdale) that show low Rb, Ba and K relative to the standard St Helena HIMU component (Sun *et al.*, 1989). These low Scottsdale values may reflect residual phlogopite left in the source. As the Scottsdale nephelinite is transitionally K-rich, retention of phlogopite in Cassidys Creek sources is minimal judging from the higher Ba and Rb in the Cassidys Creek nephelinites.

Discussion

The main features of the Cassidys Creek sequence are:

1 consistent sodic character, including the anorthoclase megacrysts,

2 co-existing melilite nephelinite and nephelinite,

3 unusual Zr/zircon relationships in evolved basalts,

4 HIMU isotopic signatures.

Sodic character. This probably marks dominant entry of amphibole over mica into the melts from the source rocks, although the role of residual phlogopite needs consideration. Experimental work on amphibole and phlogopite metasomatised peridotite showed that nephelinitic and basanitic melts can vary in Na/K contents when generated at around 28kb, depending on the precise temperature regime (Mengel & Green, 1989). At 1195°C melts have Na_2O/K_2O ratios under 1 and at 1250°C Na/K = 1, ratios less than expected for melts saturated with phlogopite. Thus, amphibole breakdown was a key process in forming these melts, while phlogopite only made a subordinate contribution and could remain in the source. However, those melts leaving residual phlogopite should show K_2O of 1.6wt% or more. This is not reached in the Cassidys Creek nephelinites or in the calculated primary basanite parent for the evolved basalts. In contrast, the Scottsdale nephelinite contains close to 1.6wt% K_2O (Frey *et al.*, 1978).

All this suggests Cassidys Creek magmas came from amphibole enriched mantle sources, in which subordinate phlogopite became consumed during melting. Hydroxy amphibole is normally stable up to 28kb and amphibole and phlogopite occur together under water saturated conditions between 25–28kb (Mengel & Green, 1989). This is the pressure range suggested for Tasmanian sodic basanite from Oatlands (Adam, 1990). However, if the melilite-nephelinite magma was generated at deeper levels than the nephelinite magmas under reduced volatile contents, then amphiboles entering melilite-nephelinite melts formed at pressures over 28kb would be F- and K-bearing amphiboles as the stable members (Foley, 1991).

Melilite-nephelinite/nephelinite relationships. The trace element patterns show the melilite nephelinite is relatively enriched in many incompatible elements including light rare earths. Its lower Fo phenocryst olivine composition also suggests a melt derived from a less magnesian-rich source. This indicates a greater metasomatised source input within the melilite-nephelinite melt than in the nephelinite melts.

The nephelinite pattern is closer to that predicted for an enriched amphibole-apatite metasomatised peridotite source (O'Reilly & Zhang, 1995), as described from Barrington, NSW, nephelinites (Fig. 9). This suggests greater amphibole incorporation into Cassidys Creek nephelinite than into the melilite nephelinite. However, less extreme depletion in Rb and K indicates more phlogopite entered the Cassidys Creek nephelinite than in the more extreme amphibole dominated Barrington nephelinites.

The fairly low and similar H_2O and CO_2 contents of both Cassidys Creek melilite nephelinite and nephelinite (around 1.4wt% total volatiles) suggest these melts were both derived from sources with modest rather than extreme volatile contents. Adam's (1990) model of differential depths of origin from sources under 7wt% volatiles is favoured, rather than melt production from sources varying in volatiles up to 14wt%. In the latter case, high H_2O and CO_2 might be expected as found in some melilite nephelinites (e.g., H_2O 4.5wt%, CO_2 2.9wt%; Herchenberg volcano, East Eiffel; Bednarz & Schmincke, 1990). However, one problem here is the quick loss of such volatiles during Herchenberg eruptions to give CO_2, H_2O poor members, so that the original source character can be lost.

Zirconium/zircon relationships. The low Zr relative to Mg# in the evolved magmas is a puzzling feature. One explanation is a restricted fractionation process in these magmas, such as previously proposed for some Tasmanian alkaline lavas (Wilkinson, 1977) and for feldspathoidal mugearites in the New England basalt field (Wilkinson & Hensel, 1991). This implies derivation of magmas from a metasomatised peridotite mantle source, giving less mafic and higher Fe/Mg primary magmas as starting points for further fractionation. It could explain the difficulty in deriving these evolved magmas by conventional fractionation processes, as utilised in the MAGFRAC program. Although a primary basanite can be modelled by adding wehrlite mineralogy from cumulates in a nepheline mugearite, these cumulates are rare at Cassidys Creek and may only represent a minor fractionation process.

A scheme that requires a highly metasomatised, amphibole-dominated mantle source to produce more "evolved" sodic primary melts is feasible given the sodic "amphibole metasomatised" nature of the sources suggested by the high Na/K and Zr in the older nephelinites. The high Zr found in the nephelinites could even come from the sodic amphiboles, as such amphiboles are capable of accommodating over 4wt% ZrO_2 (Pearce, 1989). Small volume "evolved" felsic melts forming at depth would also be rich in Na and Zr and could crystallise the anorthoclase and zircon found as megacrysts in later more voluminous "evolved" lavas. Such coarse intrusive veins would not record fractionation processes, which would explain lack of Eu depletion in the zircon megacrysts.

Preliminary uranium-lead isotope dating of Cassidys Creek zircon megacrysts give U-Pb ages between 20.6±4.8 and 12.8±4.6 Ma with the most accurate age at 15.3±1.7 Ma (F.L. Sutherland & P.D. Kinny, unpublished data). This places zircon formation at an early stage of Cassidys Creek "evolved" magmatism (14.2±0.1–13.9±0.7 Ma; Tables 1 & 2), compatible with early melting in the source region.

HIMU relationships. The Cassidys Creek sequence includes the typical HIMU isotopic source signature of Tasmanian alkaline volcanic rocks. This HIMU signature is also found in plume related basalts formed off the Tasmanian east coast and in the Balleny Islands (Ross Sea) as part of the Balleny plume system (Green, 1992; Lanyon *et al.*, 1993; Sutherland, 1994). The plume signature, besides its HIMU isotopic character, shows trace element ratios that include low La/Nb and low large ion lithophile element/Nb ratios. This plume signature appears in some east Tasmanian basalts with ages related to migratory lithospheric passage past the Balleny plume system which is now sited near Antarctica. The question arises whether the Cassidys Creek sequence shows any influence of this Tasman (Balleny) plume line and represents magmatism related to its peripheral path.

Key incompatible element ratios for Cassidys Creek rocks, eastern Tasmanian basalts (both earlier and similar ages to Cassidys Creek lavas), Balleny plume basalts and HIMU oceanic islands are compared in Table 13. The older east Tasmanian basalts fall in the Balleny plume range, but the younger east Tasmanian and Cassidys Creek lavas fall outside the range. However, all these Tasmanian basalts lie within the HIMU oceanic island range.

Thus, although sharing HIMU characteristics, not all Tasmanian alkaline basalts share the Balleny plume imprint. This is in keeping with eruption of the Cassidys Creek sequence (26–9 Ma), when Tasmania had largely migrated past the Tasman (Balleny) plume line and was entering into the domain of the separate Coral Sea-Cato Trough-North Tasmania plume system (Sutherland 1991, 1994, 1996). The precise relationships of these plume systems to the Tasmanian basalts remain for further study. However, many of the east Australian lava fields are now related to Oceanic Island Basalt (OIB) sources (O'Reilly & Zhang, 1995) and zircon megacryst generation appears to reflect plume migrations (Sutherland, 1996).

ACKNOWLEDGMENTS. The Electron Microscope Unit, University of Sydney, provided the main electron microbe facilities for mineral analysis, with some facilities provided by the School of Earth Sciences, Macquarie University through N.J. Pearson and S.Y. O'Reilly. The Tasmanian Mines Department Laboratories provided the main chemical analytical facilities, with J. Bedford and S.E. Shaw, Macquarie University, providing extra facilities. Associate Professor T.H. Green, Macquarie University and Dr. W.D. Birch, Museum of Victoria, and two anonymous referees commented on the script. W.L. Matthews published with permission of the Director, Tasmanian Division of Mines.

The late L.R. Raynor and A. Ewart, Geology Department, University of Queensland, provided electron microprobe data on a nepheline mugearite and olivine melilitite nephelinite respectively. R.E. Pogson, Division of Earth Sciences, Australian Museum, assisted with fieldwork, CIPW norm and geothermometry calculations. K. Hollis helped with the fieldwork. The Australian Museum Trust and an anonymous Friend of the Mineral Section helped in funding travel, age-dating and analytical work. S. Folwell, A. Justo and J. Howarth typed the script.

References

Adam, J., 1990. The geochemistry and experimental petrology of sodic alkaline basalts from Oatlands, Tasmania. Journal of Petrology 31: 1201–1223.

Baillie, P.W., 1986. Radiometric ages for Circular Head and the Green Hills basalt, north-western Tasmania. Unpublished Report Department of Mines Tasmania, 1986/39.

Bednarz, U. & H.-U. Schmincke, 1990. Evolution of the Quaternary melilite-nephelinite Herchenberg volcano (East Eifel). Bulletin of Volcanology 52: 426–444.

Brey, G. & D.H. Green, 1977. Systematic study of liquidus phase relationships in olivine melilitite+H_2O+CO_2 at high pressures and petrogenesis of an olivine melilitite magma. Contributions to Mineralogy and Petrology 61: 141–162.

Brown, A.V. & M.P. McClenaghan, 1982. Tertiary basaltic rocks. **In** M.P. McClenaghan, N.J. Turner, P.W. Baillie, A.V. Brown, P.R. Williams & W.R. Moore. Geology of the Ringarooma-Boobyalla area. Geological Survey of Tasmania Bulletin 61: 92–114.

Campbell, I.H. & R.W. Griffiths, 1992. The changing nature of mantle hotspots through time: Implications for the chemical evolution of the mantle. The Journal of Geology 92: 497–523.

Draper, D., 1992. Spinel lherzolite xenoliths from Lorena Butte, Simcoe Mountains, Southern Washington State (USA). The Journal of Geology 100: 766–776.

Everard, J.L., 1984. Appendix A. Petrography of Tertiary basalt, altered dolerite and tuff samples. Pp. 29–41. **In** A.B. Gulline. Geological atlas 1:50,000 Series Sheet 83 (8412N) Sorell. Explanatory Report Geological Survey of Tasmania.

Everard, J.L., 1989. Appendix B. Petrology of the Tertiary basalt. Pp. 79–142. **In** D.B. Seymour. Geological atlas 1:50,000 Series Sheet 36 (8015N) St. Valentines. Explanatory Report Geological Survey of Tasmania.

Ewart, A., 1989. Mineralogy and Mineral Chemistry. Chapter 5.3, Pp. 197–217. **In** R.W. Johnson *et al.*, (compl. & ed.) Intraplate Volcanism in Eastern Australia and New Zealand. Cambridge University Press, Cambridge.

Ewart, A., B.W. Chappell & M.A. Menzies, 1988. An overview of the geochemical and isotopic characteristics of eastern Australian Cainozoic volcanic provinces. Pp. 225–273. **In** M.A. Menzies & K.G. Cox (eds). "Oceanic and Continental Lithosphere: Similarities and Differences". Journal of Petrology Special Volume 1988. Oxford University Press, Oxford.

Ewart, A. & M.A. Menzies, 1989. Isotope Geochemistry. Chapter 5.5, Pp. 235–248. **In** R.W. Johnson *et al.* (compl. & ed.). Intraplate volcanism in Eastern Australian and New Zealand. Cambridge University Press, Cambridge.

Foley, S., 1991. High-pressure stability of the fluro-and hydroxy-endmember of pargasite and K-richterite. Geochimica et Cosmochimica Acta 55: 2689–2694.

Francis, D., 1987. Mantle-melt interaction recorded in spinel lherzolite xenoliths from the Alligator Lake Volcanic Complex, Yukon, Canada. Journal of Petrology 28: 569–597.

Francis, D., 1991. Some implications of xenolith glasses for the mantle sources of alkaline mafic magmas. Contributions to Mineralogy and Petrology 108: 175–180.

Frey, F.A., D.H. Green & S.D. Roy, 1978. Integrated models of basalt petrogenesis: A study of quartz tholeiites to olivine melilitites from South Eastern Australia utilizing geochemical and experimental petrological data. Journal of Petrology 19: 463–513.

Gee, R.D., 1971. Geological Atlas 1 mile series Sheet 22 (8016S). Table Cape. Explanatory Report Geological Survey Tasmania.

Geeves, P.D., 1982. The petrology, geochemistry and mineral chemistry of the basalts of the Wynyard area and the Table Cape teschenite. Unpublished B.Sc. Hons. Thesis. Department of Geology, University of Tasmania.

Green, P.F., 1985. A comparison of zeta calibration baselines in zircon, sphene and apatite. Chemical Geology (Isotope Geoscience Section) 58: 1–22.

Green, T.H., 1992. Petrology and geochemistry of basaltic rocks from the Balleny Is., Antarctica. Australian Journal of Earth Sciences 39: 603–617.

Green, D.H., A.D. Edgar, P. Beasley, E. Kiss & N.G. Ware, 1974. Upper mantle source for some hawaiites, mugearites and benmoreites. Contributions to Mineralogy and Petrology 48: 34–43.

Griffin, W.L., S.Y. Wass & J.D. Hollis, 1984. Ultramafic xenoliths from Bullenmerri and Gnotuk maars, Victoria, Australia: Petrology of a subcontinental crust-mantle transition. Journal of Petrology 25: 53–87.

Guo, J. & T.H. Green, 1989. Barium partitioning between alkali feldspar and silicate liquid at high temperature and pressure. Contributions to Mineralogy and Petrology 102: 328–335.

Guo, J., T.H. Green & S.Y. O'Reilly, 1992. Ba partitioning and the origin of anorthoclase megacrysts in basaltic rocks. Mineralogical Magazine 56: 101–107.

Hollis, J.D., F.L. Sutherland & A.J. Gleadow, 1986. The occurrence and possible origins of large zircons in alkali volcanics of eastern Australia. Pp. 565–578. **In** Crystal Chemistry of Minerals. Proceedings of the 13th International Mineralogical Association Meeting. 19–25th September 1982. Publishing House of the Bulgarian Academy of Science, Sofia.

Hollis, J.D. & F.L. Sutherland, 1985. Occurrences and origins of gem zircons in eastern Australia. Records of the Australian Museum 36: 299–311.

Hornig, I. & G. Wörner, 1991. Zirconolite-bearing ultra-potassic veins in a mantle-xenolith from Mt. Melbourne Volcanic Field, Victoria Land, Antarctica. Contributions to Mineralogy and Petrology 106: 355–366.

Johnson, R.W. & M.B. Duggan, 1989. Chapter 1.1.4. Pp. 12–13. **In** R.W. Johnson *et al.*, (compl. & ed.). Intraplate Volcanism in Eastern Australia and New Zealand. Cambridge University Press, Cambridge.

Lanyon, R., R. Varne & A.J. Crawford, 1993. Tasmanian Tertiary basalts, the Balleny plume, and opening of the Tasman Sea (southwest Pacific Ocean). Geology 21: 555–558.

Matthews, W.L., 1973. Gemstone occurrences at Sisters Creek. Technical Reports Department of Mines Tasmania 16: 13–15.

McDonough, W.F., M.T. McCulloch & S.S. Sun, 1985. Isotopic and geochemical systematics in Tertiary-Recent basalts from southeastern Australia and implications for the sub-continental lithosphere. Geochimica et Cosmochimica Acta 49: 2051–2067.

Mengel, K. & D.H. Green, 1989. Stability of amphibole and phlogopite in metasomatised peridotite under water-saturated and water-undersaturated conditions. **In** J. Ross (managing ed.). Kimberlites and Related Rocks Volume 1. Their Composition, Occurrence and emplacement. Geological Society of Australia Special Publication 14: 571–581.

Morimoto, N., 1988. Nomenclature of pyroxenes. Mineralogical Magazine 52: 535–550.

Morris, P.A., 1984. MAGFRAC: A basic program for least-squares approximation of fractional crystallisation. Computers and Geosciences 10: 437–444.

O'Reilly, S.Y. & W.L. Griffin, 1984. Sr isotopic heterogeneity in primitive basaltic rocks, southeastern Australia: correlation with mantle metasomatism. Contributions to Mineralogy and Petrology 87: 220–230.

O'Reilly, S.Y., W.L. Griffin & C.G. Ryan, 1991. Residence of trace elements in metasomatized spinel lherzolite xenoliths: a proton-microprobe study. Contributions to Mineralogy and Petrology 109: 98–113.

O'Reilly, S.Y. & M. Zhang, 1995. Geochemical characteristics of lava-field basalts from eastern Australia and inferred sources: connections with the subcontinental lithospheric mantle? Contributions to Mineral and

Petrology 121: 148–170.
Pearce, N.J.G., 1989. Zirconium-bearing amphiboles from the Igaliko Dyke Swarm, South Greenland. Mineralogical Magazine 53: 107–110.
Rock, N.M.S., 1991. Lamprophyres. Blackie, Glasgow.
Sack, R.O., D. Walker & I.S.E. Carmichael, 1987. Experimental petrology of alkalic lavas: constraints on cotectics of multiple saturation in natural basic liquids. Contributions to Mineralogy and Petrology 96: 1–23.
Seck, H.A., 1971. Koexistierende Alkaifeldspate und plagioclase im system $NaAlSi_3O_8$ -$KAlSiO_3$-$CaAlSi_2O_8$-H_2O bei temperaturen von 650°C. Neus Jarhbuch Mineralogie Abhandlungen 115: 315–345.
Sun, S.-s. & W.F. McDonough, 1989. Chemical and isotopic systematics of oceanic basalts: implications for mantle composition and processes, Pp. 313–346. **In** A.D. Saunders & M.J. Norry (eds). Magmatism in the Ocean Basins. Geological Society of London Special Publication 42.
Sun, S.-s., W.F. McDonough & A. Ewart, 1989. Four component model for East Australian basalts. Chapter 7.7. Pp. 333–347. **In** R.W. Johnson *et al.*, (compl. and ed.) Intraplate Volcanism in Eastern Australia and New Zealand. Cambridge University Press, Cambridge.
Sutherland, F.L., 1984. Cainozoic basalts. Pp. 103–120. **In** S.M. Forsyth, Geological atlas 1: 50,000 Series Sheet 68 (8313S) Oatlands. Explanatory Report Geological Survey of Tasmania.
Sutherland, F.L., 1985. Cainozoic volcanic rocks (Tb). **In** Farmer, N., Geological atlas 1: 50,000 Series Sheet 88 (8311N) Kingborough. Explanatory Report Geological Survey of Tasmania.
Sutherland, F.L., 1989a. Cainozoic volcanic rocks, Pp. 48–60. **In** S.M. Forsyth, Geological atlas 1: 50,000 Series., Sheet 61 (8313N), Interlaken. Explanatory Report Geological Survey of Tasmania.
Sutherland, F.L., 1989b. Tasmania and Bass Strait. Chapter 3.8, Pp. 143–149. **In** R.W. Johnson *et al.* (compl. and ed.) Intraplate Volcanism in Eastern Australian Volcanism. Cambridge University Press, Cambridge.
Sutherland, F.L., 1991. Cainozoic volcanism, eastern Australia: a predictive model based on migration over multiple 'hotspot' magma sources. **In** M.A.J. Williams, P. DeDecker & A.P. Kershaw (eds). The Cainozoic in Australia: A Reappraisal of the Evidence. Geological Society of Australia Special Publication 18: 15–43.
Sutherland, F.L., 1994. Tasman Sea evolution and hotspot trails, Pp. 35–51. **In** G.J. Van der Lingen, K.M. Swanson & R.J. Muir (eds). Evolution of the Tasman Sea Basin. A.A. Balkema, Rotterdam.
Sutherland, F.L., 1996. Alkaline rocks and gemstones, Australia: A review and synthesis. Australian Journal of Earth Sciences 43(3): 323–343.
Sutherland, F.L., A. Ewart, L.R. Raynor, J.D. Hollis & W.D. McDonough, 1989. Tertiary basaltic magmas and the Tasmanian lithosphere. **In** C.F. Burrett & E.L. Martin (eds). Geology and Mineral Resources of Tasmania. Geological Society of Australia Special Publication 15: 386–398.
Sutherland, F.L., J.D. Hollis & L.M. Barron, 1984. Garnet lherzolite and other inclusions from a basalt flow, Bow Hill, Tasmania. Pp. 145–160. **In** J. Kornprobst, J. (ed.). Kimberlites II: The Mantle and Crust-Mantle Relationships, Developments in Petrology 11B. Elsevier, Amsterdam.
Sutherland, F.L. & P. Wellman, 1986. Potassium-Argon ages of Tertiary volcanic rocks, Tasmania. Papers and Proceedings of the Royal Society of Tasmania 120: 77–86.
Wells, P.R.A., 1977. Pyroxene thermometry in simple and complex systems. Contributions to Mineralogy and Petrology 62: 129–139.
Wilkinson, J.F.G., 1977. Petrogenetic aspects of some alkali volcanic rocks. Journal and Proceedings of the Royal Society of New South Wales 110: 117–138.
Wilkinson, J.F.G. & H.D. Hensel, 1991. An analcime-mugearite-megacryst association from northeastern New South Wales: implications for high-pressure amphibole-dominated fractionation of alkaline magmas. Contributions to Mineralogy and Petrology 109: 240–251.
Wilkinson J.F.G. & R.W. LeMaitre, 1987. Upper mantle amphiboles and micas and TiO_2, K_2O and P_2O_5 abundances and $100Mg/(Mg+Fe^{2+})$ ratios of common basalts and andesites: implications for modal mantle metasomatism and undepleted mantle compositions. Journal of Petrology 28: 37–73.
Witt-Eicksen, G. & H.A. Seck, 1991. Solubility of Ca and Al in orthopyroxene and spinel peridotite: an improved version of an empirical geothermometer. Contributions to Mineralogy and Petrology 106: 431–439.
Wolff, J.A., 1987. Crystallisation of nepheline syenite in a subvolcanic magma system: Tenerife, Canary Islands. Lithos 20: 207–223.
Wood, B.J. & S. Banno, 1973. Garnet-orthopyroxene and orthopyroxene-clinopyroxene relationships in simple and complex systems. Contributions to Mineralogy and Petrology 42: 109–121.

Accepted 28 June 1996.

Appendix

Table 1. K-Ar Age Determinations, Cassidys Creek Volcanic Rocks. * Denotes radiogenic ^{40}Ar. Whole rock ages in Ma with error limits ± I.S.D. Constants used ^{40}K = 0.01167 atom %, $\lambda\beta = 4.962\times10^{-10}y^{-1}$, $\lambda\varepsilon = 0.581\times10^{-10}y^{-1}$. Age determinations by A. Webb, Amdel Report G7800/89.

Sample	%K	$^{40}Ar^*(\times10^{-11}$ moles/g)	$^{40}Ar^*/$ ^{40}Ar total	Age
Olivine nephelinite	1.14	5.2319	0.885	26.4±0.2
(mariolitic host)	1.13			
Olivine melilite nephelinite	1.125	5.1690	0.927	26.3±0.3
(from Sutherland & Wellman, 1986)	1.124			
Nepheline mugearite	2.09	5.1541	0.896	14.2±0.1
(Irbys Road flow)	2.07			

Table 2. Fission track age determinations, Cassidys Creek zircons. Coloured Group (4 grains) and Pale Group (6 grains) Standard (RHO D) and induced (RHO I) track densities measured on mica external detectors (g = 0.5), and fossil track densities on internal mineral surfaces. Total tracks counted over both groups were RHO D (2699), RHO S (1059) and RHO I (2433). Ages were calculated using = 87.7 for dosimeter glass U3 (Green, 1985). Determinations by P.F. Green, Geotrack International, Geology Department, University of Melbourne (Report No.65 held in the Australian Museum).

Sample No.	Colour Group & Range	RHO D $\times10^6cm^{-2}$	RHO S $\times10^6cm^{-2}$	RHO I $\times10^6cm^{-2}$	U ppm av(range)	Age (Ma)
8722-34	Pink-orange-red	0.632	2.453	4.737	348(193-441)	13.9±0.7
	Pale	0.632	0.599	1.689	134 (30-281)	9.5±0.6

Table 3. Representative mineral analyses, olivine melilite nephelinite. Cationic formulae are based on 6 oxygens (pyroxenes), 14 oxygens (melilite), 32 oxygens (nepheline and spinel) and 26 oxygens (sodalite and apatite). Analyses based on determinations from A. Ewart, University of Queensland, using electron microprobe facilities in the Geology Department, University of Melbourne.

Analysis	Diopside		Melilite		Nepheline	Magnetite	Sodalite	Fluor
wt%	(core)	(rim)	(core)	(rim)	(K-rich)	ulvospinel	(Cl-rich)	-apatite
SiO_2	48.98	51.51	42.94	43.19	42.98	0.14	39.68	0.76
TiO_2	2.62	1.41	0.15	0.05		21.00	0.08	
Al_2O_3	3.72	1.01	6.81	6.64	32.68	0.54	30.66	
Cr_2O_3	0.15	0.06	0.06			0.59		
"FeO"	5.83	5.30	4.19	4.06	0.96	69.95	1.04	0.31
MnO	0.13	0.17	0.06			0.88		
MgO	13.84	14.84	7.16	7.52		2.96		
CaO	24.43	24.49	33.45	34.31	0.11	0.07	0.12	54.39
Na_2O	0.46	0.57	4.33	4.07	15.70	0.11	20.89	
K_2O			0.05	0.09	6.87	0.01	0.19	
P_2O_5								39.46
Cl,F							Cl 7.82	F 3.26
							0≡Cl 1.76	0≡F 1.37
Total	100.16	99.36	99.20	99.93	99.30	96.25	98.72	96.81
Si^{4+}	1.827	1.926	3.942	3.938	4.188	0.024	6.381	0.133
Ti^{4+}	0.073	0.040	0.010	0.004		2.596	0.010	
Al^{3+}	0.164	0.045	0.736	0.714	3.752	0.104	5.811	
Cr^{3+}	0.004	0.002	0.004			0.076		
Fe^{2+}	0.182	0.166	0.322	0.310	0.080	9.612	0.140	0.045
Mn^{2+}	0.004	0.005	0.004			0.124		
Mg^{2+}	0.769	0.827	0.980	1.022		0.724		
Ca^{2+}	0.976	0.981	3.290	3.352	0.012	0.012	0.023	10.188
Na^{1+}	0.033	0.041	0.770	0.720	2.964	0.036	6.513	
K^{1+}			0.006	0.010	0.852	0.004	0.039	P5.840
							Cl 2.131	F 1.802
Σ cations	4.032	4.033	10.064	10.070	11.848	13.312	21.046	18.008
	Wo 49.5	Wo 49.2	Ca 80.9	Ca 82.1	Ne 78.5	Usp 59.5	Na 75.0	Ca 57.1
	En 42.9	En 42.5	Na 18.9	Na 17.6	Ks 16.9	Mt 20.8	K 0.4	P 32.8
	Fs 7.6	Fs 8.3	K 0.2	K 0.3	Q 4.6	Mf 17.6	Cl 24.6	F 10.1
						Hc 1.2		
						Cm 0.9		

Table 4. Representative mineral analyses, olivine nephelinite. Cationic formulae are based on 4 oxygens (olivine), 6 oxygens (pyroxenes), 32 oxygens (nepheline and feldspar) and 24 oxygens (amphiboles and micas). Analysed totals are normalised for anhydrous phases for closer comparison with totals for hydrous phases. Analysts D.F. Hendry and B.J. Barron. * May represent the presence of BaO.

Analysis	Olivine		Diopside		Nepheline	Anorthoclase	Ti-mica	Amphibole
wt%	(large)	(small)	(large)	(small)	(grdmass)	(grdmass)	(grdmass)	(grdmass)
SiO_2	40.37	38.52	47.71	49.70	44.50	65.41	37.67	46.74
TiO_2	0.04		2.50	2.85		0.31*	8.71	1.23
Al_2O_3	0.14		4.81	3.76	33.09	20.62	11.81	9.13
Cr_2O_3			0.35					
"FeO"	11.55	20.91	5.96	6.34	0.82	0.31	10.14	7.63
MnO	0.21	0.39	0.09	0.14				0.17
MgO	47.50	39.83	13.20	13.76			15.70	16.41
CaO	0.09	0.35	23.76	22.61	0.59	1.49	1.46	13.45
Na_2O	0.05		1.61	0.90	16.92	7.33	0.40	1.79
K_2O	0.04		0.01		4.08	4.53	7.72	0.29
Total	99.99	100.00	100.00	100.00	100.00	100.00	93.61	96.84
Si^{4+}	0.998	0.997	1.791	1.849	8.484	11.656	6.105	7.060
Ti^{4+}	0.001		0.071	0.080			1.061	0.140
Al^{3+}	0.004		0.213	0.165	7.440	4.332	2.258	1.624
Cr^{3+}			0.011					
Fe^{2+}	0.239	0.453	0.187	0.197	0.132	0.044	1.374	0.964
Mn^{2+}	0.004	0.008	0.003	0.005				0.020
Mg^{2+}	1.749	1.536	0.738	0.760			3.791	3.692
Ca^{2+}	0.003	0.010	0.955	0.902		0.284	0.253	2.176
Na^{1+}	0.003		0.117	0.065	6.252	2.532	0.126	0.524
K^{1+}	0.001		0.001		0.992	1.028	1.597	0.056
Σ cations	3.002	3.003	4.087	4.023	23.420	19.876	16.565	16.256
	Fo 87.9	Fo 77.1	Wo 49.3	Wo 47.8	Ne 83.8	Ab 65.9	Mg 60.9	Mg 54.0
	Fa 12.1	Fa 22.9	En 50.1	En 44.6	Ks 9.4	Or 26.7	Fe 22.1	Fe 14.1
			Fs 0.6	Fs 7.6	Q 5.5	An 7.4	Ti 17.0	Ca 31.9

Table 5. Representative mineral analyses, nepheline mugearite. Cationic formulae based on 4 oxygens (olivine), 6 oxygens (pyroxenes), 32 oxygens (feldspar and zeolite). Analyses B.J. Barron. * May represent presence of BaO.

Analysis	Olivine		Diopside		Anorthoclase		Sanidine	Zeolite
wt%	(phenocryst)	(grdmass)	(core)	(rim)	(grdmass)	(vein)	(grdmass)	(vein)
SiO_2	39.37	35.95	51.05	48.31	63.53	64.49	65.38	48.50
TiO_2	0.09		1.04	1.72	0.12*	0.23*	0.11*	0.05*
Al_2O_3	0.24	0.12	2.38	4.69	22.21	20.69	19.08	23.96
Cr_2O_3		0.01	0.10	0.22				
"FeO"	16.97	31.65	6.30	7.72	0.26	0.32	0.56	0.71
MnO	0.21	0.69	0.15	0.12		0.04	0.02	
MgO	42.90	31.16	14.71	12.95	0.02	0.13	0.07	3.00
CaO	0.20	0.33	23.66	23.50	3.26	2.25	0.12	7.21
Na_2O		0.03	0.56	0.77	7.82	7.96	6.07	0.28
K_2O	0.03	0.08	0.05	0.01	2.78	3.88	8.58	1.11
Total	100.01	100.01	100.00	100.01	100.00	99.99	99.99	84.30
Si^{4+}	0.998	0.985	1.900	1.817	11.321	11.529	11.838	10.130
Ti^{4+}	0.001		0.029	0.049	0.016	0.030	0.015	0.008
Al^{3+}	0.007	0.004	0.104	0.208	4.663	4.359	4.070	5.897
Cr^{3+}		0.002	0.003	0.007				0.005
Fe^{2+}	0.360	0.725	0.196	0.243	0.040	0.047	0.086	0.123
Mn^{2+}	0.004	0.016	0.005	0.004		0.006	0.004	
Mg^{2+}	1.620	1.271	0.816	0.725	0.005	0.037	0.019	0.932
Ca^{2+}	0.005	0.010	0.943	0.947	0.621	0.432	0.024	1.613
Na^{1+}		0.002	0.040	0.056	2.700	2.758	2.131	0.113
K^{1+}	0.001	0.003	0.002	0.000	0.630	0.083	1.981	0.295
cations	2.996	3.018	4.038	4.053	19.996	20.081	20.168	19.116
	Fo 81.8	Fo 63.7	Wo 46.6	Wo 44.0	Ab 68.3	Ab 67.7	Ab 51.5	Ca 79.8
	Fa 18.2	Fa 36.4	En 47.0	En 50.3	Or 15.9	Or 21.7	Or 47.9	K 14.6
			Fs 6.5	Fs 5.7	An 15.7	An 10.6	An 0.6	Na 5.6

Table 6. Representative phenocryst, groundmass and megacryst phases, zircon-bearing evolved lavas. Analyses normalised to 100%. Cationic formulae based on 4 oxygens (olivine), 6 oxygens (pyroxene), 32 oxygens (feldspar). Analyses D.F. Hendry and B.J. Barron. * May represent presence of BaO.

Rock	Nepheline hawaiite (Analysis 7)						Nepheline mugearite (Analysis 8)			
Mineral	Olivine		Clinopyroxene		Anorthoclase		Ol	Cpx	Anorthoclase	
wt%	core	(rim)	core	(rim)	grd-mass	mega-cryst	pheno-cryst	pheno-cryst	grd-mass	mega-cryst
SiO_2	39.96	(39.17)	50.39	(51.74)	59.42	67.29	40.08	45.67	61.48	67.42
TiO_2			1.79	(1.31)			0.02	3.45	0.15*	
Al_2O_3			3.40	(2.55)	23.99	19.89		5.95	23.36	20.01
Cr_2O_3				(0.32)		0.03	0.12			
"FeO"	15.17	(17.46)	8.63	(7.01)	0.91	0.14	12.72	9.29	1.25	0.13
MnO	0.17	(0.19)	0.14			0.24	0.15			
MgO	44.20	(42.75)	13.42	(14.41)			46.88	11.80	0.39	
CaO	0.21	(0.23)	21.63	(22.17)	0.97	0.73	0.02	22.80	2.85	0.69
Na_2O			0.58	(0.48)	10.25	9.57		0.76	7.13	9.17
K_2O	0.07				4.45	2.40		0.01	3.58	2.58
NiO	0.26	(0.20)								
Si^{4+}	1.050	(0.996)	1.883	(1.917)	10.812	11.864	0.996	1.737	11.039	12.001
Ti^{4+}			0.050	(0.036)			0.000	0.099	0.016	
Al^{3+}			0.150	(0.112)	4.136		0.267	4.943	4.198	
Cr^{3+}				(0.009)		0.001	0.004			
Fe^{2+}	0.318	(0.371)	0.270	(0.217)	0.136	0.024	0.264	0.295	0.188	
Mn^{2+}	0.004	(0.004)	0.004		0.001	0.005				
Mg^{2+}	1.657	(1.621)	0.747	(0.796)		1.736	0.668	0.103		
Ca^{2+}	0.006	(0.006)	0.866	(0.880)	0.188	0.136	0.001	0.928	0.549	0.133
Na^{1+}			0.042	(0.035)	3.616	3.272		0.056	2.481	3.164
K^{1+}	0.002				1.032	0.540		0.000	0.774	0.586
Ni^{2+}	0.006	(0.004)								
cations	3.043	(3.002)	4.012	(4.002)	20.932	19.954	2.999	4.059	20.093	20.082
	Fo 83.8	(81.3)	Wo 43.9	(43.9)	Ab 74.7	Ab 82.7	Fo 86.8	Wo 45.3	Ab 65.2	Ab 81.5
	Fa 16.2	(18.7)	En 42.8	(44.5)	Or 21.4	Or 13.7	Fa 13.2	En 43.6	Or 20.3	Or 15.1
			Fs 13.3	(11.7)	An 3.9	An 3.4		Fs 11.1	An 14.4	An 3.4

Table 7. Representative mineral analyses, mariolitic segregations, olivine nephelinite. Analyses are normalised for closer comparison, except hydrous or halogen-bearing minerals. Cationic formulae are based on 4 oxygens (olivine), 6 oxygens (pyroxenes), 32 oxygens (nepheline, feldspars), 24 oxygens (amphiboles, micas) and 26 oxygens (sodalite). Analyses D.F. Hendry and B.J. Barron.

Analysis wt%	Olivine	Augite	Na-augite	Sanidine	Nepheline	Sodalite	Ulvospinel	Amphibole	Ti-Mica
SiO_2	38.56	54.00	53.17	62.80	43.46	39.32	1.06	52.63	37.47
TiO_2		0.37	1.34		0.10		13.58	2.74	10.70
Al_2O_3		0.79	0.60	18.73	33.30	30.06	0.23	2.60	12.08
Cr_2O_3	0.40	0.10							
"FeO"	24.75	6.48	12.10	1.02	0.94	1.30	78.48	8.21	11.53
MnO	0.66	0.14	0.28		0.08		1.14	0.19	0.10
MgO	35.77	15.81	10.60		0.07		1.53	17.40	15.03
CaO	0.22	21.63	17.61		0.15			7.08	
Na_2O		0.65	4.21	2.59	15.32	22.36		5.59	0.17
K_2O		0.03	0.03	11.92	6.58	0.14		1.82	8.27
Cl						7.33			
BaO				2.94		O≡Cl 1.76			
Total	100.00	100.00	100.01	100.00	100.00	98.86	96.02	98.26	95.35
Si^{4+}	1.020	1.990	2.010	11.764	8.360	6.356	0.366	7.836	6.010
Ti^{4+}		0.010	0.040		0.020		3.540	0.303	1.290
Al^{3+}		0.030	0.030	4.134	7.550	5.727	0.094	0.459	2.280
Cr^{3+}		0.010							
Fe^{2+}	0.547	0.200	0.380	0.160	0.150	0.176	22.747	1.023	1.550
Mn^{2+}	0.013		0.010		0.010		0.334	0.021	0.010
Mg^{2+}	1.413	0.870	0.600		0.020		0.789	3.861	3.590
Ca^{2+}	0.007	0.850	0.710		0.030		1.127		
Na^{+}		0.050	0.310	0.941	5.710	7.008	1.617	0.310	0.050
K^{1+}			0.000	2.849	1.610	0.029		0.344	1.690
Cl						2.008			
Ba^{2+}				0.215					
Σ cations	3.000	4.010	4.090	20.064	23.460	21.303	27.870	16.591	16.480
	Fo 72.0	Wo 43.4	Wo 47.6	Ab 23.5	Ne 76.3	Na 77.5	Mt 48.9	Mg 64.2	K 55.8
	Fa 28.0	En 46.9	En 43.4	Or 71.1	Ks 19.4	K 0.3	Usp 42.1	Fe 17.0	Mg 24.1
		Fs 9.7	Fs 9.0	Cn 5.4	Q 4.3	Cl 22.2	Mf 8.5	Ca 18.8	Ti 20.1
							Hc 0.5		

Table 8. Representative analyses, spinel lherzolite xenoliths and reaction replacements, olivine nephelinite host. Cationic formulae are based on 4 oxygens (olivine), 6 oxygens (pyroxenes), 32 oxygens (spinel, feldspar). Analyses D.F. Hendry. CIPW norms for glasses are calculated on a volatile content basis, assuming volatiles by difference from 100% totals.

Mineral	Spinel lherzolite xenolith				Reaction phases in xenolith				
wt%	Olivine	Diopside	Enstatite	Cr-spinel	Olivine	Augite	Sanidine	Glass 1	Glass 2
SiO_2	40.75	53.02	56.30	1.14	40.50	56.40	67.53	46.84	45.67
TiO_2		0.29	0.14	0.26					0.15
Al_2O_3		4.76	3.16	47.23		0.37	17.66	10.78	13.49
Cr_2O_3		0.87	0.41	20.75		1.76			
"FeO"	9.98	2.56	6.06	9.90	10.23	3.52	1.21	2.60	5.68
MnO	0.11		0.16	0.23	0.17	0.12			
MgO	49.71	15.71	31.75	19.82	48.91	18.23	0.32	12.61	14.12
CaO		21.64	0.94	0.17	0.15	18.06		1.71	2.20
Na_2O		0.90				1.40	5.64	0.72	
K_2O						0.17	7.76	5.05	2.59
NiO	0.32				0.18				
Total	100.87	99.75	98.91	99.50	100.13	100.03	100.13	80.31	83.92
Si^{4+}	0.992	1.922	1.970	0.245	0.994	2.032	12.128	Or 30	Q 7
Ti^{4+}		0.008	0.010	0.041				Ab 6	Or 15
Al^{3+}		0.203	0.130	11.959		0.016	3.740	An 8	An 11
Cr^{3+}		0.250		3.522		0.050		C 1	C 7
Fe^{2+}	0.203	0.078	0.180	1.777	0.210	0.106	0.180	Hy 32	Hy 43
Mn^{2+}	0.002			0.042		0.004	0.004	Ol 2	Mt 1
Mg^{2+}	1.804	0.849	1.650	6.345	1.790	0.979	0.088	Mt 1	Il 0
Ca^{2+}		0.840	0.040	0.040	0.004	0.697			
Na^{1+}		0.063				0.098	1.960		
K^{1+}						0.008	1.776		
Ni^{2+}	0.006				0.003				
Σ cations	3.008	3.988	3.980	23.972	3.006	3.988	19.872	100.0	100.0
	Fo 89.9	Wo 37.7	En 88.6	Sp 79.6	Fo 89.4	Wo 33.9	Ab 52.5	Na 14.4	Na 0
	Fa 10.1	En 57.1	Fs 9.5	Cm 16.6	Fs 10.6	En 61.4	Or 47.5	K 66.7	K 58
		Fs 5.2	Wo 1.9	Usp 3.8		Fs 4.7	An 0.0	Ca 18.9	Ca 42

Table 9. Comparative olivine, pyroxene and spinel compositions, cumulate inclusions and host lherzolite-bearing nepheline mugearite. Analyses recalculated to 100% totals, with cationic formulae based on 4 oxygens (olivine), 6 oxygens (pyroxenes) and 32 oxygens (spinel). Analyses B.J. Barron.

Mineral	Spinel wehrlite			Nepheline mugearite			Megacrysts	
wt%	Ol	Cpx	Spl	Ol	Cpx	Spl	Ol	Opx
SiO_2	40.24	49.92	0.12	39.39	51.04	0.17	41.05	54.72
TiO_2	0.01	1.37	0.39	0.09	1.04	26.01	0.04	
Al_2O_3	0.12	8.30	63.60	0.24	2.38	0.42	0.01	5.10
Cr_2O_3	0.01	0.13	0.28		0.10	0.06		0.39
"FeO"	14.10	4.20	14.42	16.98	6.30	49.33	9.19	6.29
MnO	0.10	0.16	0.01	0.21	0.15	0.85	0.12	0.13
MgO	45.25	14.40	21.12	42.91	14.71	2.39	49.47	32.34
CaO	0.14	19.71	0.06	0.20	23.66	0.75	0.09	0.96
Na_2O		1.75			0.56	0.01		0.05
K_2O	0.03	0.06			0.05	0.02	0.03	0.04
Si^{4+}	1.005	1.819	0.025	0.998	1.900	0.052	1.003	1.892
Ti^{4+}		0.036	0.060	0.002	0.029	6.055	0.001	
Al^{3+}	0.003	0.357	15.259	0.067	0.104	0.149	0.003	0.208
Cr^{3+}		0.004	0.044		0.003	0.015		0.011
Fe^{2+}	0.294	0.128	2.454	0.359	0.196	17.952	0.188	0.182
Mn^{2+}	0.002	0.005	0.002	0.004	0.005	0.219	0.003	0.004
Mg^{2+}	1.683	0.782	6.405	1.620	0.816	1.104	1.800	1.665
Ca^{2+}	0.004	0.769	0.013	0.005	0.943	0.246	0.002	0.036
Na^{1+}		0.123			0.040	0.005		0.004
K^{1+}		0.003		0.001	0.002	0.007	0.001	0.002
Σ cations	2.991	4.026	24.262	3.055	4.038	25.803	3.001	4.004
	Fo 85.1	Wo 36.1	Sp 79.4	Fo 81.8	Wo 46.6	Usp 71.1	Fo 90.6	En 88.5
	Fa 14.9	En 59.9	Hc 14.9	Fa 18.2	En 47.0	Mf 15.9	Fa 9.4	Fs 9.5
		Fs 4.0	Mt 4.4		Fs 6.5	Mt 12.0		Wo 2.0
			Cm 0.3			Hc 0.9		

Table 10. Representative Analyses, Crustal Inclusions. Cationic formulae are based on 6 oxygens (pyroxenes) and 32 oxygens (feldspars). Analyses D.F. Hendry and B.J. Barron.

Mineral	Two-Pyroxene Granulite			Anorthosite
wt%	Enstatite	Diopside	Andesine	Oligoclase
SiO_2	53.94	53.11	58.00	62.25
TiO_2	0.12	0.29		
Al_2O_3	1.53	2.79	26.32	24.00
Cr_2O_3	0.16	0.25		
"FeO"	17.32	6.41		0.14
MnO	0.29			
MgO	25.75	14.20		
CaO	0.29	21.78	7.86	5.21
Na_2O		0.92	6.61	8.16
K_2O			0.33	0.62
Total	99.40	99.75	99.12	100.33
Si^{4+}	1.969	1.959	10.452	11.012
Ti^{4+}	0.003	0.008		
Al^{3+}	0.066	0.121	5.592	4.996
Cr^{3+}	0.005	0.007		
Fe^{2+}	0.529	0.198		0.020
Mn^{2+}	0.009			
Mg^{2+}	1.401	0.780		
Ca^{2+}	0.011	0.861	1.520	
Na^{1+}		0.066	2.308	2.800
K^{1+}			0.076	0.140
Σ cations	3.993	4.000	19.944	19.956
	En 72.2	Wo 42.0	Ab 59.1	Ab 71.3
	Fs 27.2	En 46.5	An 38.9	An 25.1
	Wo 0.6	Fs 11.6	Or 1.9	Or 3.6

Table 11A. Chemical Analyses, Cassidys Creek and Table Cape Basalt Suites.

Major Elements	1	2	3	4	5	6	7	8	9
SiO_2	38.77	40.49	42.51	44.46	46.63	47.37	47.15	47.00	47.26
TiO_2	3.34	2.81	2.26	2.00	1.62	1.82	1.73	1.71	1.81
Al_2O_3	8.75	8.92	12.61	13.25	13.77	14.62	13.85	14.12	14.39
Fe_2O_3	5.22	6.42	7.07	4.41	3.92	5.02	3.18	3.77	3.56
FeO	7.87	6.62	6.61	9.34	7.25	6.12	7.76	7.93	7.71
MnO	0.21	0.19	0.19	0.18	0.18	0.18	0.17	0.23	0.20
MgO	12.56	13.75	8.92	9.63	8.56	6.70	7.04	7.98	7.09
CaO	14.72	12.42	8.81	8.47	7.44	7.36	8.04	7.22	7.19
Na_2O	3.89	3.94	4.42	3.85	5.98	4.61	5.07	6.48	6.00
K_2O	1.34	1.10	1.87	1.53	2.12	2.16	2.37	2.14	2.44
P_2O_5	1.56	1.21	1.20	0.70	0.84	0.88	0.86	0.81	0.84
H_2O	1.18	1.29	2.75	2.14	2.08	2.86	2.62	1.20	1.60
CO_2	0.24	0.18	0.35		0.10	0.16	0.12		
Total	99.65	99.34	99.57	99.35	100.49	99.86	99.96	100.59	100.09
C.I.P.W. norm									
Or			11.41	9.30	12.73	13.16	14.39	12.73	14.64
Ab			10.57	14.96	15.69	25.25	18.81	15.20	17.06
An	2.49	3.47	9.34	14.77	4.54	13.22	8.25	3.14	5.20
Lc	6.31	5.20							
Ne	18.11	18.42	15.20	10.05	19.35	8.11	13.69	21.66	18.68
Di	30.49	37.48	20.79	19.78	21.79	14.32	21.43	22.55	20.84
Ol	21.93	22.38	21.15	22.33	17.82	17.13	15.02	16.73	15.35
Mt	3.21	3.21	3.41	3.24	2.74	2.78	2.72	2.84	2.77
Il	6.44	5.44	4.43	3.91	3.13	3.56	3.38	3.27	3.49
Ap	3.75	2.92	2.94	1.71	2.02	2.15	2.09	1.93	2.02
Cc	0.55	0.42	0.82	–	0.23	0.38	0.28	–	–
Cs	6.79	1.11	–	–	–	–	–	–	–
D.I.	24.4	23.6	37.2	34.3	47.8	46.5	46.9	49.6	50.4
An%	100.0	100.0	46.9	49.7	22.4	34.4	30.5	17.1	23.4
Mg value	0.673	0.693	0.582	0.612	0.621	0.563	0.579	0.594	0.574
Na_2O/Na_2O+K_2O	0.74	0.78	0.70	0.72	0.74	0.68	0.68	0.75	0.71
Na_2O+K_2O/Al_2O_3	0.60	0.57	0.50	0.41	0.59	0.46	0.53	0.61	0.59
$ASI(Al_2O_3/CaO+Na_2O+K_2O)$	0.44	0.51	0.83	0.96	0.89	1.03	0.89	0.89	0.92

Table 11B. Trace elements.

ppm	1	2	3	4	5	6	7	8	9
Ni	246	390	230	278	240	165	155	210	160
Cr	548	650	320	325	320	220	220		
Co		63	53		46	47	43		
Sc		25	12	16	15	11	13		
V	238	240	165	165	125	145	140		
Ba	516	250	165	165	125	145	140	200	210
Zr	452	370	330	201	410	410	410	390	430
Y	43	32	23	19	22	22	22	24	22
Sr	1296	1050	1350	794	1000	1750	960	970	1150
Rb	23	24	20	9	18	19	27	17	17
Nb	120	96	82	44	87	86	83		
La	105	84	65	31	45	47	39		
Ce	192	165	150	66	120	120	115		
Nd	98	50	41	32	29	30	27		
Zn	127	135	175		160		150	165	155
Cu	85	96	125		62	63	56	43	34
Sn		<4	13		7	6	5		
W		70	115		54	72	36		
Bi		6	5		5	<5	<5		
Mo		5	10		6	8	8		
As		29	20		22	20	24		
Th	11	<4	4	3	7	<4	8		
U	<2	<5	5	<1	<5	<5	<5		
Pb	20	5	9		5	<4	<4		
Ga	22	15	25		27	26	26		
Zr/Nb	3.77	3.85	4.02	4.57	4.71	4.77	4.94		
Sr/Rb	56.3	43.8	67.5	88.2	55.6	92.1	35.5	47.1	67.6
Ba/Rb	22.4	10.4	8.3	18.3	6.9	7.6	5.2	11.8	12.4
Sr/Ba	2.5	4.2	8.2	4.8	8.0	12.1	6.9	4.9	5.5
Rb/Nb	0.19	0.25	0.24	0.20	0.21	0.22	0.33		

1. Olivine melilite nephelinite (block), north Cassidys Creek (8235E, 6690N).
2. Olivine nephelinite (block), north Cassidys Creek (8235E, 6685N).
3. Nepheline hawaiite, north Cassidys Creek (8240E, 6690N).
4. Nepheline hawaiite, (flow base), south Table Cape (9316E, 6506N).
5. Anorthoclase-nepheline mugearite (flow), north Cassidys Creek (8236E, 6685N).
6. Nepheline hawaiite (block), north Cassidys Creek (8235E, 6690N).
7. Anorthoclase-nepheline hawaiite (block), north Cassidys Creek (8235E, 6690N).
8. Anorthoclase-nepheline mugearite (block), north Cassidys Creek (8235E, 6690N).
9. Anorthoclase-nepheline mugearite (flow), north Cassidys Creek (8245E, 6680N).

Analysis 1. School of Earth Sciences, Macquarie University, Sydney (J. Bedford).
Analyses 2–3, 5–9. Tasmanian Department of Mines (Nos. 872732–972737, 850242–850243).
Analysis 4. Geology Department, University of Queensland (A. Ewart).

Table 12. Petrographic details, basalt types, Cassidys Creek.

Rock Type	Texture	Phenocrysts	Groundmass
Olivine-melilite nephelinite (Analysis 1)	microporphyritic, rock includes mantle debris	olivine (Mg_{84}), melilite ($Ca_{71\text{-}72}$ Mg_{21} $Fe_{6\text{-}7}$)	zoned Al-Ti diopside (Ca_{50} Mg_{42} Fe_{8}), melilite (Ca_{71} Mg_{22} Fe_{7}), nepheline (Na_{78} K_{22}), interstitial sodalite (Na_{75} $K_{0\text{-}1}$ $Cl_{24\text{-}25}$), ulvospinel
Olivine-nephelinite (Analysis 2)	glomeroporphyritic, rock includes mantle debris	olivine ($Mg_{89\text{-}92}$) diopside (Mg_{39} $Ca_{50}Fe_{10}$), rims (Mg_{37} Ca_{51} Fe_{12})	olivine, clinopyroxene, ulvospinel, nepheline, zoned alkali feldspar. Segregations of nepheline ($Na_{84\text{-}88}$ $K_{10\text{-}14}$ $Ca_{1\text{-}2}$), anorthoclase ($Na_{56\text{-}66}$ $K_{26\text{-}27}$ $Ca_{7\text{-}5}$)
	mariolitic cavity, prismatic crystals up to 4.5 mm projecting inwards from margins towards an irregular central cavity	diopside ($Mg_{44\text{-}46}$ $Ca_{44\text{-}47}$ $Fe_{9\text{-}11}$) in radiating prisms zoned to sodian augite ($Mg_{35\text{-}38}$ $Ca_{42\text{-}45}$ $Fe_{20\text{-}30}$) and partly altered to Ti richterite ($Mg_{64\text{-}71}$ $Ca_{16\text{-}19}$ $Fe_{12\text{-}17}$), subhedral nepheline ($Na_{77\text{-}81}$ $K_{19\text{-}22}$ $Ca_{0\text{-}1}$), zoned sanidine ($K_{74\text{-}80}$ $Na_{20\text{-}26}$) tablets, radiating groups and intergrowths including Ba sanidine (K_{71} Na_{24} B_5), sodalite (Na_{78} Cl_{22}) overgrown on pyroxenes and containing aegirine augite (?), accessory ulvospinel ($Fe_{79\text{-}85}$ $Ti_{12\text{-}17}$ $Mg_{2\text{-}5}$), Ti phlogopite ($Mg_{55\text{-}56}$ $Fe_{23\text{-}25}$ $Ti_{20\text{-}25}$), apatite, ilmenite. Intersertal glass, radiating feldspathic mesostastasis and a botryoidal carbonate filling.	
Nepheline-hawaiite (Analysis 3)	aphyric rock, includes mantle debris		olivine, prismatic clinopyroxene, stumpy to poikilitic subhedral nepheline, zoned and simply twinned feldspar, scattered ulvospinel.
Nepheline-hawaiite (Analyses 6 & 8)	microporphyritic, anorthoclase and zircon xenocrysts, crustal debris	zoned olivine (Mg_{84}) with rims ($Mg_{81\text{-}69}$)	zoned sodic plagioclase, nepheline, alkali feldspar, scattered ulvospinel. Mariolitic cavities with prismatic diopside (Mg_{38} Ca_{47} Fe_{15}), mosaic anorthoclase ($Na_{74\text{-}75}$ $K_{21\text{-}22}$ Ca_{4}), minor nepheline and zeolitic amygdales.
Nepheline-Mugearite (Analysis 5)	microporphyritic, anorthoclase xenocrysts, mantle debris	zoned olivine ($mg_{83\text{-}71}$), rare zoned diopside ($Mg_{37\text{-}42}$ $Ca_{47\text{-}50}$ $Fe_{10\text{-}13}$)	olivine (Mg_{63}), clinopyroxene needles, zoned sodic feldspar ($Na_{63\text{-}68}$ $K_{16\text{-}22}$ $Ca_{10\text{-}16}$) interstitial sanidine ($Na_{51\text{-}52}$ $K_{47\text{-}48}$ $Ca_{0\text{-}1}$) scattered ulvospinel (Fe_{74} Ti_{24} Mg_{4}).
Nepheline mugearite (Analyses 8 & 9)	microporphyritic, anorthoclase and zircon xenocrysts, crustal debris	olivine (Mg_{87}) Al-Ti augite ($Mg_{35\text{-}34}$ $Ca_{49\text{-}50}$ $Fe_{15\text{-}16}$)	olivine, clinopyroxene, ulvospinel, nepheline ($Na_{90\text{-}91}$ $K_{8\text{-}9}$ $Ca_{0\text{-}1}$), poikilitic anorthoclase ($Na_{65\text{-}66}$ $Ca_{14\text{-}15}$ $K_{20\text{-}21}$), yellow glass.

Table 13. Incompatible trace element ratios, Tasmanian, Balleny Plume and HIMU basalts.

Basalt Group	Zr/Nb	La/Nb	Ba/Nb	Ba/Th	Rb/Nb	K/Nb	Ba/La
Cassidys Creek nephelinites	3.7–3.9	0.88	2.6–4.3	47–63	0.19–0.25	93–95	3.0–4.9
Table Cape ne hawaiite	4.6	0.70	2.0	55	0.20	289	5.3
NE Tasmanian nephelinite	3.3	0.64	2.6	38	0.12	133	4.0
NE Tasmanian alkali basalt	3.6	0.53	5.2	73	0.37	156	9.7
Balleny Plume basalts	3.1–4.6	0.57–0.62	5.0–7.2	64–99	0.32–0.72	111–216	9.3–12.6
HIMU oceanic islands	0.4–5.6	0.07–0.85	1.0–8.2	23–151	0.01–0.45	13–266	2.4–15.4

Cassidys Creek/Table Cape ratios from this paper. NE Tasmanian nephelinite ratios from Frey *et al.* (1978). NE Tasmanian alkali basalt ratios from Sutherland (1989b) and A.E. Ewart unpublished data. Balleny plume basalt and HIMU oceanic island basalt ratios from Lanyon *et al.* (1993).